MICROSTRUCTURAL AND MECHANICAL CHARACTERIZATION OF NITROGEN ION IMPLANTED AND PLASMA ION NITRIDED PLASTIC INJECTION MOULD STEEL

By

Ortaç ONMUŞ

A Dissertation Submitted to the
Graduate School in Partial Fulfillment of the
Requirements for the Degree of

MASTER OF SCIENCE

Department: Materials Science and Engineering
Major: Materials Science

İzmir Institute of Technology
İzmir, Turkey

August, 2003

We approve the thesis of **Ortaç ONMUŞ**

Date of Signature

_____ 26.08.2003

Assoc. Prof. Dr. Orhan ÖZTÜRK
Supervisor
Department of Physics

_____ 26.08.2003

Assoc. Prof. Dr. Mustafa GÜDEN
Co-Supervisor
Department of Mechanical Engineering

_____ 26.08.2003

Prof. Dr. Ahmet ÖZTARHAN
Tübitak Textile Research Center, Ege University

_____ 26.08.2003

Prof. Dr. Muhsin ÇİFTÇİOĞLU
Department of Chemical Engineering

_____ 26.08.2003

Assoc. Prof. Dr. Mehmet GÜNEŞ
Department of Physics

_____ 26.08.2003

Prof. Dr. Muhsin ÇİFTÇİOĞLU
Head of Interdisciplinary
Material Science and Engineering Program

ACKNOWLEDGEMENTS

I am very grateful to my advisor, Assoc. Prof. Dr. Orhan Öztürk, for his invaluable help, guidance, and encouragement as well as his self-sacrifice and understanding provided during this thesis.

I would like to thank my co-advisor, Assoc. Prof. Dr. Mustafa Güden, for suggestions and valuable discussions besides his very interesting and nice graduate courses.

This study presented here satisfies one of the aims of a larger research and development project (Tübitak-Tidep #3000249) directed by Prof. Dr. Ahmet Öztarhan who is presently affiliated with Tübitak Textile Research Center, Ege University, İzmir. Special appreciation is therefore, extended to Prof. Dr. Ahmet Öztarhan, for providing me the opportunity to study in the project and to use the facilities in Yüzey Teknolojileri Corporation.

Prof. Dr. D. L. Williamson, Colorado School of Mines, Golden, CO USA is acknowledged for performing the Mössbauer spectroscopy measurements.

I also would like to thank Beşok Kalıpçılık for providing materials for the plasma nitriding and nitrogen ion implantation and Dönmez Debriyaj for the salt spray corrosion analysis.

I would like to acknowledge my institution, İzmir Institute of Technology, for providing me research facilities during my graduate study.

Special thanks go to research assistants in our institution for their help and friendship during my graduate study.

Finally I wish to express my gratitude to my family, especially to my lovely wife, for their continuing, encouragement, support, and patience during the course of my studies here at Iztech.

ABSTRACT

In this study, high-chromium ferritic plastic injection mould steel (X36CrMo17, similar to AISI-420F) was subjected to plasma nitriding and nitrogen ion beam implantation under various conditions. The effectiveness of conventional plasma nitriding and nitrogen ion beam implantation conditions in improving the tribological properties and mechanical performance was investigated.

The experimental results clearly show that plasma nitriding and nitrogen ion beam implantation lead to the development of the various near-surface microstructures and enhanced mechanical properties.

Plasma nitriding was performed at a temperature range between 520-540 °C, with a bias voltage of 500 V for 15 to 18 hours under various gas mixtures of N_2+H_2 in an industrial nitriding facility (micro-pulsed DC). Nitrogen ion beam implantation was carried out with $2x10^{17}$ and $1x10^{18}$ ion doses with an 85 kV nitrogen ion energy at temperatures ≤ 200 ˚C.

Near-surface phases, compositions, plasma nitrided and nitrogen implanted layer thicknesses and the strength of these layers were studied by a combination of symmetric (θ-2θ) and grazing incidence x-ray diffraction (XRD and GIXRD), conversion electron and x-ray Mössbauer spectroscopies (CEMS and CXMS), cross-sectional scanning electron microscopy (SEM) and cross-sectional nanohardness measurements. The corrosion behaviour was investigated by a salt spray method and by observation of acid etching during SEM sample preparation. The tribological properties (friction and wear) were examined by a ball-on-disc tribometer.

Combined Mössbauer, XRD, and SEM analyses clearly indicate that (Fe,Cr,Mn)-nitrides and CrN are distributed in the top nitrided layers of several micron thickness. The CEMS and CXMS analyses show the nearly complete decomposition of the near surface and deeper crystal structures into pure bcc α-(Fe), (Fe,Cr,Mn)-nitrides, consisting of ε-Fe_3N and γ´-Fe_4N, and CrN. The XRD, CEMS and CXMS results also show an Fe_3C-like carbide phase, $(Fe,Cr,Mn)_3C$, in the nitrided layers, whose presence is attributed to C segregation to the near-surface region and to extra carbon being present in the nitriding system.

The nitriding conditions with the gas composition N_2/H_2=1 produces the thickest nitrided layer (about 135 μm) with an excellent resistance to corrosion. The nanohardness measurements indicate that the cross sectional hardness-depth profiles under all nitriding conditions is found to be plateau-shaped, and the nitrided layer surface hardness values are found to be increased by a factor of about three in

comparison to that of the substrate material. This study also showed that the hardening effect in plasma nitrided specimens was due to a fine and homogeneous chromium nitride precipitation. The wear analysis results showed that the nitrided layers have reduced friction coefficient values (20 to 25%) and possess excellent wear resistance in comparison to that of the bulk material.

It was also found that nitrogen ion implantation into plastic injection mould steel produces N content rich layers (less than 0.1 μm thick) with enhanced wear and corrosion properties. The surface nanohardness measurements of the low and high dose implanted specimens indicate that the hardness values increase by factors of about 1.4 and 1.6, respectively, compared to the substrate material. The salt spray corrosion analysis (2% NaCl solution in distilled water) experiments showed enhanced corrosion behaviour for the N implanted layers, and that nitrogen ion implantation is a viable method for improving corrosion resistance of plastic injection mould steel.

Combined Mössbauer and XRD data reveal that the N implanted layers consist of ε-nitride phase, ε- $(Fe,Cr,Mn)_{2+x}N$, with both magnetic (x~1) and paramagnetic (x~0) characteristics. Based on the CEMS results, the N implanted layer thicknesses are found to be ~ 40 and 65 nm for the low dose ($2x10^{17}$ ions/cm^2) and high dose ($1x10^{18}$ ions/cm^2) dose N implanted specimens, respectively.

ÖZ

Bu çalışmada, ferritik yapıya sahip yüksek krom alaşımlı plastik enjeksiyon kalıp çeliğine (X36CrMo17, AISI-420F çeliğine benzer yapı ve alaşımdadır) değişik şartlar altında plazma nitrasyon ve azot iyonu implantasyonu yapılmıştır. Kullanılan bu metodların optimizasyonunu sağlamak için malzemelerin yüzey özellikleri ve mekanik peformansları üzerindeki etkileri araştırılmıştır.

Deneysel sonuçlar plazma nitrasyon ve azot iyonu implantasyonunun malzemelerin yüzeylerinde gelişmiş mekanik özelliklere sahip çeşitli mikroyapıların oluşumuna yol açtığı göstermiştir.

Malzemeler değişen oranlarda N_2+H_2 gaz karışımları kullanarak 500 V sabit polarizasyon gerilimi ve 520 ila 540 ºC işlem sıcaklıkları altında 15 ila 18 saat arasında değişen sürelerde mikro titreşimli doğru akım üreteçli endüstriyel bir cihaz ile plazma nitrasyon işlemlerine tabi tutulmuşlardır. Azot iyon implantasyonu ise 200˚C'den düşük sıcaklık seviyesinde 85 kV hızlandırma gerilimi altında $2x10^{17}$ ve $1x10^{18}$ doz oranları kullanılarak gerçekleştirilmiştir.

Yüzey faz ve mikroyapıları, plazma nitrürlenmiş ve azot implantasyonu yapılmış tabakaların kalınlıkları ve bu tabakaların sertlikleri simetrik (θ-2θ) ve anti simetrik x-ışınları kırınımı (XRD ve GIXRD), dönüşüm elektronu ve x-ışınları Mössbauer spektroskopileri (CEMS ve CXMS), elektron mikroskobu (SEM) ve nanosertlik ölçümleri aracılığı ile karakterize edilmiştir. Malzemelerin paslanma özellikleri başta "tuz püskütme testi" olmak üzere elektron mikroskobu için malzeme hazırlanması sırasında asit ile dağlanmaları ile araştırılmış, tribolojik özellikler (sürtünme ve aşınma) ise malzeme üzerinde aşındırıcı-top kullanma yöntemi ile incelenmiştir.

Mössbauer, XRD ve SEM analiz sonuçları (Fe,Cr,Mn)-nitrürlerin ve CrN'ün nitrürlenmiş tabakanın birkaç mikrometre kalınlığındaki en üst tabakasında dağılım halinde olduğunu göstermiştir. CEMS ve CXMS analizleri yüzeyden belli derinliğe kadar olan tabakalarda bulunan kristal yapıların neredeyse tamamen, içinde ε-Fe_3N, γ′-Fe_4N, ve CrN gibi fazları bulunduran (Fe,Cr,Mn)-nitrürlere ve saf bcc α-(Fe)'e ayrıştığını göstermiştir. Ayrıca XRD, CEMS ve CXMS sonuçları Fe_3C-benzeri bir karbür'ün [$(Fe,Cr,Mn)_3C$] nitrürlenmiş tabakalarda oluştuğunu ortaya koymuştur. Bu oluşumun sebebi yüzey tabakalarına karbon birikmesine ve/veya nitrürleme sisteminin içinde bulunan ekstra karbon varlığına dayandırılmıştır.

N_2/H_2 = 1 gaz karışımı ile yapılan plazma nitrürleme işleminin en kalın nitrürlenmiş tabakanın oluşumuna yol açtığı (yaklaşık olarak 135 μm) ve bu tabakanın çok yüksek paslanma dayanımına sahip olduğu gözlenmiştir. Malzemenin yan kesitinden yapılan nano-sertlik

ölçümleri ile sertlik dağılımının bütün malzemelerde birbirlerine benzer olarak bir plato bölgesi oluşturduğu ve yüzey sertlik değerlerinin işlem görmemiş malzemeye göre 3 kat kadar artmış olduğu belirlenmiştir. Bu çalışmada ayrıca malzemelerde görülen sertlik artışının sebebinin küçük homojen tanecikli CrN çökelti fazı oluşumu olduğu bulunmuştur. Sürtünme ve aşınma deneyleri, plazma nitrürlenmiş yüzeylerin düşük sürtünme katsayılarına (%20 ila %25 oranında) ve aşınmaya yüksek dayanıma sahip olduklarını açığa çıkarmıştır.

Plastik enjeksiyon kalıp çeliğine yapılan azot iyon implantasyonu sonucu bu malzemelerin yüzeyinde aşınma ve paslanma dayanımı yüksek, azot miktarı açısından zengin tabakaların (yaklaşık olarak 0.1 μm kalınlığında) oluştuğu bulunmuştur. Düşük ($2x10^{17}$ ions/cm^2) ve yüksek ($1x10^{18}$ ions/cm^2) dozda yapılan implantasyon sonrasında yapılan yüzey sertlik ölçümleri malzemelerin yüzey sertliklerinin ham malzemeye kıyasla sırasıyla, en az 1.4 ve 1.6 kat kadar arttığını göstermiştir. Tuzlu su püskürtme yoluyla yapılan paslanma analizi ölçümleri (%2'lik NaCl barındıran saf su çözeltisi) azot iyon implantasyonu yapılan tabakaların gelişmiş paslanma dayanımına sahip olduğunu ve iyon implantasyonunun kullanılan plastik enjeksiyon kalıp çeliğinin paslanma direncinin arttırılması için uygun bir yöntem olduğu göstermiştir.

Mössbauer ve XRD analizi azot implante olmuş tabakaların ε-nitrür, ε- $(Fe,Cr,Mn)_{2+x}N$ gibi fazları barındırdığını ve bu fazların hem manyetik (x~1) hem de paramanyetik (x~0) özellikler taşıdığını ortaya koymuştur. CEMS analizi ise düşük ve yüksek dozda azot implante edilmiş tabakaların sırasıyla ~40 and 65 nm kalınlıklarında olduğunu göstermiştir.

TABLE OF CONTENTS

LIST OF FIGURES

LIST OF TABLES

CHAPTER 1

INTRODUCTION

1.1 General Background

Plastic mould steels, a new generation of tool steels, are of great industrial importance. For the simple reason that the use of plastics for daily life is increased and so there is a great demand for steels for plastic processing. The area of application extends from components for the plastic-processed industry like extruder screws to components for foodstuffs, chemistry, medical industry and it finds a growing need in replacing many other materials used in daily life [1]. Therefore, the requirements on plastic mould steels are very different. Over the years, manufacturing techniques and alloy compositions have been developed, modified and refined to meet an expanding demand for specific physical and chemical properties. The progress in plastic mould tool steel development, on the other hand, has been dictated not only by demands of the user industries, but also by the economic considerations: larger series and shorter cycle times are required to produce good and constant product quality at low production costs.

Today, there will be an increasing need to limit the use of the most sophisticated steels and to develop systems which allow the use of cheap materials for the bulk properties, while focusing specialized properties into those areas where they are required. This introduces the concept of "Surface Engineering" which enables the surface of the steel to be modified to produce specific properties. It has been recognised for several years that tribological problems (friction, wear, and lubrication) in the production of plastics are mainly concentrated in the following areas [1] and significantly reduce the functionality and the lifetime of many vital plastic moulds (PM) and components:

- Adhesive wear and galling of toll-part surfaces due to reciprocating cyclic movement,

- Abrasion from the flow of molten plastics,
- 60Corrosion of tool surfaces due to corrosive exhaust gases or decomposition products from the plastics,
- Release problems on the surfaces in contact with plastics,
- Filling problems of small cavities on the surfaces of the moulds.

These tribological problems may be solved by an appropriate use of vacuum-based surface treatments and may bear no relation to the properties required by the bulk material, which are more controlled by the properties of the surface of materials [1-3].

The existence of many different tools and components, made from different metals and steels, which might be hardened and tempered differently and be able to withstand different temperature ranges triggered the emergence of a wide range of vacuum-based surface treatments, tackling about these tribological problems. Among the best known are plasma nitriding (PN), ion implantation (II), physical vapour deposition (PVD), or plasma chemical vapour deposition (PCVD). These techniques have very different characteristics such as different process temperatures, and influence the work piece differently, and also the application areas are rather different [1-4].

Plasma nitriding and ion implantation are advanced surface modification techniques, which have been put into use and successfully introduced as commercial surface treatments for several tool types for over a decade [1-4].

1.2 Plasma nitriding

Plasma nitriding process is a development of the traditional gas nitriding process and is a thermochemical surface treatment used in steel and alloys to improve wear and friction properties by introducing nitrogen ions into the surfaces where they are required. The basic principle of plasma nitriding is as follows: if two electrodes of differing potential are placed in a gas in a reduced pressure and an increasing negative bias voltage is applied, at a certain minimum voltage a glow is set up a few centimetres around the electrode of lower potential. Plasma nitriding is carried out in the region of abnormal glow discharge where the work piece to be nitrided is completely covered with glow [5] and due to the interaction between the ionised nitrogen in the plasma and the surface of the work piece, nitrogen starts to diffuse into the specimen. The absorbed nitrogen forms a nitrogen-rich environment, which is named as nitrided layer or zone. If

the nitrogen content in the surface is high enough, nitrides will be precipitated. The result, basically, is a two-layer structure. The outer layer is a hard iron nitride compound (or white layer) layer and the inner layer is a slightly softer diffusion layer [5,6]. Good tribological anticorrosion properties are ascribed to the compound layer, whereas improvement of the fatigue resistance is due to the diffusion zone [7-9].

Phase transformations during nitriding are dependent on the nitrogen content diffused into the ferritic matrix during the thermochemical treatment. According to iron-nitrogen phase diagram [10] the nitrogen solubility limit in ferrite is 0.1% in mass. The increase in nitrogen content leads to nitride precipitation. The equilibrium iron nitrides in the Fe-N system are γ'-Fe_4N, which has ordered fcc structure, and ε-$Fe_{2-3}N$, which has hexagonal structure with magnetic and paramagnetic characteristics [11,12].

Although the mechanical improvement of the surfaces of the nitrided steels is due to the interaction of nitrogen with the steel and the change in the microstructure as a result of nitrogen diffusion, in most nitriding treatments hydrogen is also used in combination with nitrogen since it is known that the addition of hydrogen has a beneficial effect on the nitriding process [13]. Kumar *et al*. [14] investigated the effect of hydrogen on the growth of the nitrided layer in r.f.-plasma nitrided austenitic stainless steel and concluded that the addition of hydrogen in the range between 5-50% to an otherwise pure nitrogen plasma results in an increased nitrided-layer thickness while an excessive amount of hydrogen in the gas mixture (> 50%) retards the nitriding process. In addition to hydrogen and nitrogen gas mixtures, alternative mixtures such as nitrogen+argon, nitrogen+hydrogen+neon, and combination of these are used to enhance the rate of nitriding in the plasma nitriding process. In one such study [15], the role of hydrogen and argon on plasma nitriding of a low-alloy steel (AISI 5140) was investigated. This study showed that the amount of Ar in dual gas mixtures must be at least 20% to obtain distinctive hardness values.

The response of steels or alloys to plasma nitriding is not only derived from process parameters, such as time, temperature, bias voltage, and gas mixtures, but it is highly dependent on the steels or alloy compositions [16]. Alloy elements in steel affect the nitriding response, mainly when nitride forming elements are present. Alloy elements such as Al, Ti, Cr, V, and Mo interact differently with nitrogen and directly affect the nitriding response, mainly regarding surface hardening properties [17]. The growth and the compositional profile of the nitrided layers was studied for various Fe-

Cr alloys consisting of 5, 10 and 20 wt. % Cr [18] under a fixed N_2/H_2 = 1/4 gas flow ratio and a nitriding temperature of about 500 °C for 1-8 hours. Under these conditions, CrN, γ'-Fe_4N and ε-$Fe_{2-3}N$ phases were observed and the nitrided layer thicknesses were found to depend on the Cr concentration. This study finds that an increase in the amount of Cr results in a decrease in the thickness of the nitrided layers due to the selective bonding between Cr and N. They further showed that the thickness of the nitrided layer increases with an increase in nitriding time.

Another investigation was carried out on various ferritic grades of steel by Berg *et al.* [6] from N_2/H_2 = 1/4 to pure N_2. The nitriding conditions for this study included the following: (1) a bias voltage of 500 V; (2) nitriding temperatures ranging between 500-560 °C for 15 hours. The steels used in this investigation were construction steel (CS) with no Cr, nitriding steel (NS) with low Cr (1.5-1.8 wt.%), and tool steel (TS) with high amount of Cr (8.0 wt.%). This study showed that the formation of a compound layer is verified under all nitriding conditions in the CS steel. In the NS steel, the compound layer formation is observed when the N_2/H_2 ratio, the voltage or the nitriding time was increased. However, in the TS steel, which is similar to the steel in our study, the compound layer formation is not observed under all process conditions. The thickness of the compound layer is found to be dependent on the process parameters changing from 0 to 12 μm and from 1 to 11 μm in the NS and the TS steels, respectively.

Plasma nitriding and nitrogen ion implantation induce nitride formation, which contributes to an increase in the surface hardness for the plasma nitrided and ion-implanted layers. One research study, by Pinedo *et al.* [19] deals with the effects of plasma nitriding on surface hardening mechanism(s). In this study, a martensitic grade high chromium steel, which is quite similar in composition to the steel used in our study, and is also used in plastic injection moulding was subjected to plasma nitriding at temperatures ranging from 480-560 °C and at a gas mixture of N_2/H_2 = 3/1 and under a bias voltage of 470 V for 4 hours. Under these processing conditions, the presence of a compound layer was verified for all nitriding temperatures. The nitrided specimens show a strong hardening effect, up to 4 times in comparison to that of the bulk material, with the formation of a maximum hardness plateau. The most important finding for this study is the plateau-shaped hardness profiles. This flat type hardness profile is attributed to the strong interaction characteristics of the Cr with nitrogen and represents the

nitrogen compositional profile through the nitrided layer, in high chromium ferritic alloy steels.

Most of the plastic moulds suffer from wear due to low surface hardness and high friction coefficients as explained in the previous section. Many studies [20,21] focused on the wear behaviour and the service life of plasma nitrided tool steels and demonstrated that friction coefficient of the steels can be decreased while the wear resistance is increased and as a result, the service life of the tool steel can be increased up to 2-3 times depending on the particular material and the process parameters of the nitriding.

It is known that the compound layers with iron nitrides have good corrosion resistances. This is found to be the case for the plasma nitriding study of an X20Cr13 ferritic stainless steel material (quite similar to the one investigated in this study) which showed that the plasma nitrided layer with monophase, ε-Fe_3N (ε-nitride phase) has a very good corrosion resistance, which was investigated by the ferri/ferro-cyanide test [22]. And an improvement in corrosion resistance could not be observed for the plasma nitrided steel with multiphase (ferrite and γ'-Fe_4N) compared to the untreated material. The focus of this research, in which nitriding time, N_2/H_2 gas-flow ratio and bias voltage were varied in order to produce different diffusion profiles, was to study the effect of the nitrided layer on the formation and performance of subsequent Ti-C:H coatings.

1.3 Nitrogen Ion Implantation

Ion implantation was first used in semiconductor industry to introduce controlled dopants into the semiconductor materials. Metal alloys formed by ion-beam methods have been studied since the 70`s [2-4]. These studies use ion implantation to inject elements directly into a target. This method produces atomic scale alloys, as opposed to mechanical mixtures of the species. This alloyed region is denoted as implanted layer or zone. Numerous ion species, both gaseous and metallic such as N, C, B, Si, Fe, Cr, Ti, and even inert ions such as Ar or He have been implanted into steels. Among them nitrogen is the most widely studied element with respect to others, due to the fact that the surfaces implanted with nitrogen results in improved tribological properties such as wear, and fatigue resistances and even corrosion resistance [1-4,23-26].

Conventional ion implantation is a low temperature treatment [3,4]. (The substrate temperatures are near ambient.) The typical energies and the ion beam current densities used in the ion implantation studies are in the range between 20 to 200 keV and a few $\mu A/cm^2$, respectively. The elements are, therefore, alloyed together by athermal ballistic processes, which may allow some of the thermodynamic and kinetic constrains which usually govern alloy formation to be bypassed. This advantage permits metastable compositions and structures to be more readily achieved, although thermodynamic and kinetic considerations still determine alloy microstructures [27]. One of the main drawbacks of the ion implantation is the shallowness of the implanted layer, which is ≤ 0.1 μm [4,27]. This thin implanted layer might be a problem for applications requiring wear resistant surfaces. In addition, the line-of-sight character of ion implantation can make it impossible to introduce implanted ions into the regions with complex geometries.

Today there are a number of ion implantation based methods using elevated temperatures (~350-600 °C), high ion beam current densities (100 to 5000 $\mu A/cm^2$) and/or complicated treatments such as: plasma immersion ion implantation, (PI^3) or fast pulsing, low voltage plasma immersion ion implantation, ($FLPI^3$) [28,29]. These conditions produce much thicker nitrogen implanted layers with lots of nitrogen in them resulting in better wear and corrosion resistances and load bearing capacities. But still, conventional ion beam implantation has its niche in the sector [1-4] of tooling industry due to the fact that the treatment can be applied to finished products with no change in dimensions and can improve the mechanical properties of the substrate while capable of enhancing tribological and mechanical properties.

High energy, high flux nitrogen ion beam implantation has been investigated by Williamson *et al.* [30] and it was concluded that nitrogen ion implantation into pure iron (α-Fe) typically results in iron-nitrides, Fe_xN, with compositions x and structures that fall into three categories: (1) x near 2 with hexagonal (ε) or orthorhombic (ξ) crystal structures which are nonmagnetic; (2) x near 3 with ε-structure which is magnetic; (3) x=4 with the ordered fcc (γ′) structure which is magnetic.

The influence of nitrogen ion implantation on the tribological properties of a high chromium tool steel (12 wt.%), which is similar to one investigated in our study, was studied by Budzyński *et al.* [31]. The steel specimens were subjected to nitrogen ion implantation under various energies ranging from 8.5-120 keV and to ion doses

(ions/cm^2) ranging from 1x10^{16}–4.3x10^{17} at room temperature. In this study, the friction and the wear properties of the N implanted layers were investigated by a pin-on-disk tribometer. It was found that the nitrogen ion implantation with a dose higher than 1x10^{17} ions/cm^2 induces a reduction in the friction coefficient (μ) and increases resistance to wear, while the lower doses causes no significant changes to the same properties.

The influence of N ions to the wear and fatigue resistance of ion-implanted layers have been studied extensively but the results are rather confusing. One such study [32], concluded that the ion implantation improves wear and friction properties while the others [33,34] conclude that no significant improvement in these properties is achievable. To answer these questions, detailed hardening mechanisms were investigated by Kliauga *et al.* [35]. In this study, a high-chromium ferritic and an austenitic steel were N ion implanted with energies of 60 and 100 keV, under doses ranging from 1x10^{17} to 1x10^{18} ions/cm^2. It was demonstrated that the hardening of the implanted surfaces was caused by the increase of interstitial atoms in the austenite (solid solution hardening) and by combination of nitrogen with Cr and/or Fe leading to the precipitation of nitrides in the ferrite. This study also indicated that the nitride precipitation in the ferritic steel contributed to the reduction of wear rate, yet its effect on reducing fatigue was not representative as in the austenitic steel.

Another implantation study [36] involving both nitrogen and nitrogen+carbon ion implantation into a ferritic cold-work steel (12 wt.% Cr) by plasma immersion ion implantation (PI^3) showed that nitrogen ion implantation at a dose of 6x10^{17} N/cm^2 followed by carbon ion implantation at a dose of 1.8x10^{18} C/cm^2 at a temperature 350 ºC is the optimum treatment condition for reducing both the wear resistance and friction coefficient. The implanted layer in this study was composed of ε-$Fe_{2+x}N$ [or ε-$Fe_{2+x}(NC)$] and had a thickness of 3 μm. The results also showed that a two-layer structure of compound and diffusion layer was obtained similar to that observed at higher temperatures or conventional plasma nitriding conditions. This study demonstrated that combination of nitrogen implantation (which reduces abrasive wear) with carbon (which reduces the friction coefficient) is suitable for the cases where complex wear mechanisms occur.

1.4 Purpose of This Work

The main objective of this research is to improve our understanding of surface modification of chromium plastic injection mould steels with nitrogen ion implantation and plasma ion nitriding processes. In particular, surface mechanical properties such as hardness, wear, friction and corrosion behaviour of the nitrided and N ion implanted layers under various N_2+H_2 gas compositions and nitrogen ion doses will be investigated, respectively.

This will be accomplished by experimental characterization of the near-surface crystal structures and the N-implanted and the nitrided layer thicknesses and strengths using a combination of symmetric and grazing incidence x-ray diffraction (XRD and GIXRD), conversion electron and x-ray Mössbauer spectroscopies (CEMS and CXMS), cross-sectional scanning electron microscopy (SEM) and cross-sectional nanohardness measurements.

The results of this research should lead to an understanding of the effects of plasma nitriding conditions and nitrogen ion beam conditions on the development of various near-surface crystal structures and surface mechanical improvements of plastic injection mould steels.

CHAPTER 2

EXPERIMENTAL METHODS

2.1 Plasma Nitriding

An X36CrMo17 (AISI ~ 420F) prehardened plastic injection mould steel (an FeCr ferritic stainless steel) was the base material onto which surface modification is applied. The chemical composition of the material is given in Table 2.1.

Table 2.1. Chemical composition (all in wt %) of ferritic plastic injection mould steel used in this study.

AISI	German Standard	Symbol	C	Si	Mn	Cr	S	Fe
~420F	1.2316	X36CrMo17	0.33	0.35	1.35	16.7	0.07	81.2

For plasma ion nitriding and nitrogen ion implantation, disk-like specimens were chosen having 3.00 cm in diameter and 0.40 cm in thickness. This geometry was specifically designed for friction and wear analyses before and after the surface modification treatments. The average grain size for the specimens of this study, estimated by metallography was ~ 30-60 μm. Before all the treatments the specimens were polished down to a mirror-like quality with an average surface roughness of 0.02 μm based on surface profilometry.

The nitriding experiments were performed in an industrial plasma nitriding facility, Rubig, micro-pulsed DC plasma nitriding unit. A schematic representation of the essential elements of the micro-pulsed plasma ion nitriding unit is shown in Fig. 2.1. The advantage of micro-pulsed systems is that it allows better control of temperature and suppresses arcing [37]. After cleaning in alcohol, the polished specimens were placed into the plasma-nitriding chamber connecting with the cathode and then the chamber was evacuated. Before the nitriding step, the passive oxide film was removed

by high-density pure hydrogen sputtering for 45 min under a temperature of 525 °C, a bias voltage of 520 V, and a pressure of 10 mbar. After the sputtering step is completed, the chamber is evacuated again and then is filled with predetermined nitrogen and hydrogen gas mixtures. The specimens were subjected to plasma nitriding under various nitrogen-hydrogen gas flow ratios, (N_2/H_2), based on volumetric gas flow per hour, for 15 to 18 hours under a temperature range, a bias voltage, and a working pressure of, 520 to 540 °C, 500 V, and 2-3 mbar, respectively. The applied bias voltage then ionizes the mixture and a glow is set up around cathodised specimens. The charged ions (within a few centimeters of the work piece) are accelerated and hit the surface with a relatively high level of kinetic energy. A large proportion of this energy is transferred to heat. The plasma thereby heats the work piece to its required nitriding temperature. In this study, the temperature of the nitrided specimens was measured by chromel–alumel thermocouples attached to the back of the samples. The much smaller part of the kinetic energy of the ions is used to release atoms out of the metal lattice (sputtering). Not only metallic elements, such as iron and/or chromium, are released, but also non-metallic elements such as carbon, nitrogen, hydrogen.

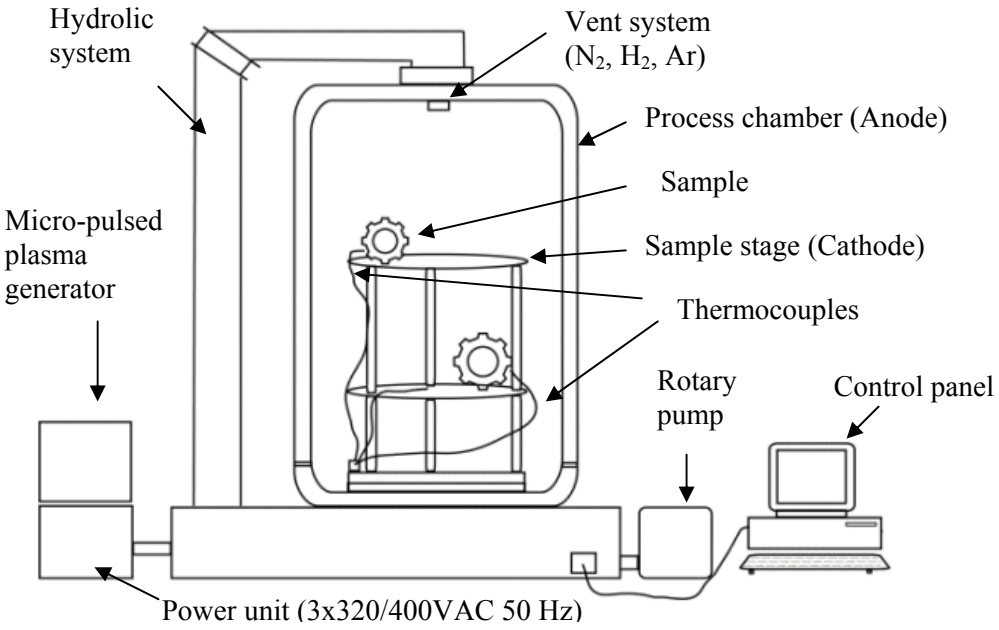

Figure 2.1. A schematic drawing indicating the essential elements of the micro-pulsed plasma ion nitriding unit.

The specimens plasma nitrided (a total of 10 for the nitriding experiments) prepared for this research and the micro-pulsed plasma ion nitriding parameters are given in Table 2.2.

Table 2.2. Plasma nitriding process conditions.

Specimen No	Gas Flow Ratio (N_2/H_2)	Temperature (°C)	Time (h)
SC10, SC11, SC12	1/10	520	15
SC3, SC4, SC5, SC6	1/1	540	18
SC13, SC14, SC15	3/1	520	15

2.2 Nitrogen Ion Implantation

In addition to plasma ion nitriding, the surfaces of the plasma injection mould steel (AISI ~ 420F) was also modified by nitrogen ion implantation. The implantation was carried out by an industrial type of broad beam low current density ion beam implanter (Implant Sciences). A schematic diagram and the essential elements of the implantation system are given in Fig. 2.2. Before placing the samples on to the specimen stage, the specimens went through the polishing and cleaning procedure explained in the previous and later sections for the nitriding treatment and the care was taken not to contaminate the samples after the cleaning procedure. The nitrogen ion beam conditions included the following:

(1) an accelerating voltage of 85 keV;

(2) nitrogen doses of $2x10^{17}$ and $1x10^{18}$ ions/cm^2;

(3) implantation times of 8 and 20 h.

The chamber pressure during the implantation was $4x10^{-5}$ torr. In this system, the beam (not mass analysed) is established via introducing nitrogen gas through ion source and is ionised by the application of a bias voltage. The sample stage was designed to rotate radially to decrease the line-of-sight restrictions of the ion implantation during the process. One handicap of this system is that it hinders measuring the temperature of the specimens during the treatment directly via thermocouples. No external heating takes place during the treatment and the temperature of the specimens depends on the current density of the ion beam. The system, on the other hand, is known as conventional implantation system running under

a temperature range of less than 200 °C [3] (we believe that the temperature is estimated to be less than or equal to 100°C due to low current density of the ion beam used by the system). The nitrogen ion implanted specimens for this research (a total of 6) and the implantation process conditions are summarized in Table 2.3. Note that the beam current in the table refers to the total ion beam current in the system thus, the current on the specimen is much smaller. We estimated that the current density of the ion beam used by the system is ≤ 1 μA/cm^2.

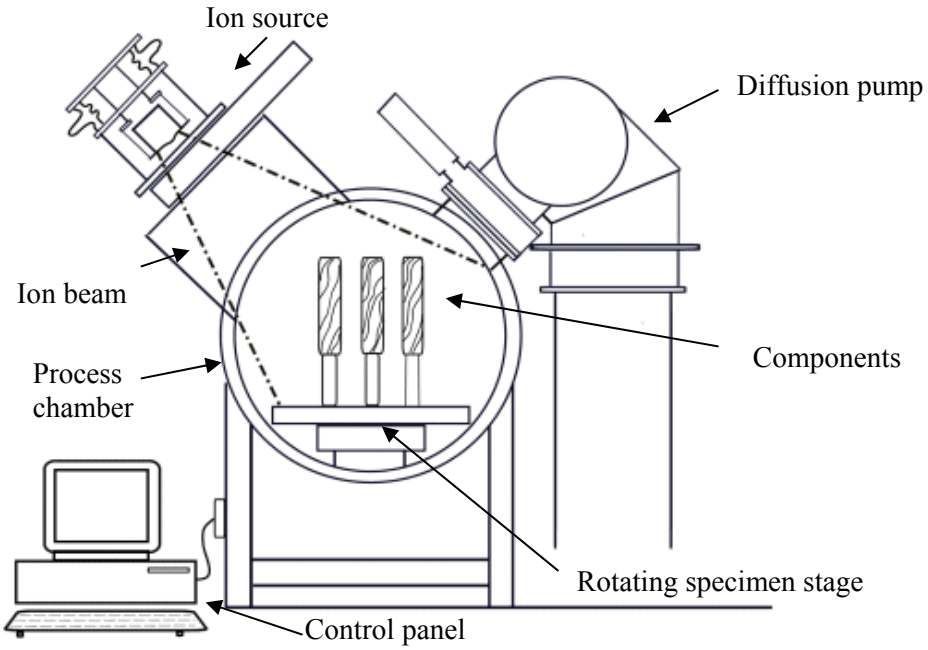

Figure 2.2. A schematic drawing indicating the essential elements of the implantation system.

Table 2.3. Nitrogen ion implantation conditions.

Specimen No (SC)	Dose (ions/cm^2)	Process Time (h)	Beam Current (mA)
SC7, SC8, SC9	2 x 10^{17}	8	12
SC16, SC17, SC18	1 x 10^{18}	20	11

2.3 Microstructure Characterization Techniques

Near-surface phases, compositions, plasma nitrided and nitrogen implanted layer thicknesses of the specimens were mainly characterized by x-ray diffraction (XRD) and scanning electron microscopy (SEM). In addition, energy dispersive x-ray spectroscopy

(EDX) and optical microscopy (OP) were also used to provide information on selected samples. To gain further insight about the microstructure, the information provided by conversion electron Mössbauer spectroscopy (CEMS) and conversion x-ray Mössbauer spectroscopy (CXMS) in backscattering mode was also evaluated.

2.3.1 XRD Analysis

X-ray diffraction can be used for characterization of near surface layers since low energy x-rays are strongly absorbed in passing through the solid material. The fundamental physical and chemical knowledge obtained by this analysis may be classified as: chemical composition and crystal structure determination, layer composition and thickness determination.

The XRD measurements were made with a θ / 2θ diffractometer with Cu Kα x-rays (λ=1.541 Å for the 8.05 keV x-rays) from a high intensity x-ray generator (Philips Expert). The typical operating voltage and current used were 45.0 kV and 40.0 mA, respectively. The data collection was made with a computer-controlled system. The resultant spectrum (diffractogram) is in the form of the scattered x-ray intensity (counts/s) versus 2θ (degrees). The presented diffractograms in this study were plotted in square root of x-ray intensity [Sqrt (counts/sec)] versus 2θ (degrees) to reveal weaker patterns much more clearly. The 2θ range for the specimens of this study was between 30 to 100 degrees, which gives a scan time of about 1 hour 56 minutes for the step widths and times used in this experiment (0.05° and 4.00 s, respectively). The experimental XRD data were evaluated using the available software. The first step in the process is to locate the peak positions and then the search-match method is performed to identify the peaks that are present.

The effective depth probed by Cu Kα x-ray (which can be calculated from $\sin\theta/2\mu$ [7] where μ is the effective linear absorption coefficient and approximately equals to 0.23 μm^{-1} for X36CrMo17 steel used in this study) was such that it allowed the characterization of the top nitrided and nitrogen implanted layers as well as the substrate phase. Two different geometries: (1) Bragg-Brentano (XRD) and (2) grazing incidence x-ray diffraction geometry (GIXRD) are facilitated during the XRD measurements.

2.3.1.1 Bragg-Brentano Method

This method generally is known as powder method, and can be defined as a symmetric method since the system always detects the scattered x-rays at a diffraction angle which is equal to the angle of x-rays incident on the surface. Both the sample and the detector move step by step during the measurement. While the sample rotates at an angle the detector moves two times this angle. This method, therefore, always detects the diffracted x-rays from grains oriented parallel to the surface, not the others. Figure 2.3a shows the basic geometry of this system. One disadvantage of this geometry is that the effective depth probed by the incident beam always changes during the scan due to the change in the angle of the incident beam. For example, a typical scan range in 2θ for most metals is between 30 to 100 degrees. Due to change in the incident beam angle, the effective depth probed by the beam at $2\theta = 100$ degree is approximately 3 times deeper than the effective depth probed by the beam at $2\theta = 30$ degrees. This property of the method might cause some misinterpretation if it is not taken notice on examining for example, a material having a layered-structure. This introduces the concept of fixing the angle of the incident beam and scanning the scattered beam. For those kind of analysis the following method will be considered.

2.3.1.2 Grazing Incidence X-Ray Diffraction (GIXRD)

In this system, the incident x-ray beam is fixed to a predetermined value on the sample and detector scans 2θ degrees. Different from the powder method, this method facilitates diffraction from the planes not parallel to surface, never the parallel ones. Normally this method uses a very small angles incident on the surface allowing providing information from quite thin layers and is ideally suitable for examination of typical implantation modified layer thicknesses which is on the order of 0.1 μm. The main power behind this method, therefore, involves providing the information layer by layer by just changing the angle of x-ray beam incident on the sample surface since the effective depth probed by the fixed x-ray beam incident on the sample is mainly dependent on this angle [~ $\sin\omega/\mu$- For incident angle ω and exit angle β, $2\theta=\omega+\beta$, then effective depth is $(1/\mu)=((1/\sin\omega)+(1/\sin\beta))^{-1}$, which for very small ω is approximately $\sin\omega/\mu$ [7]]. Due to extremely low incident angles the scattered beam mainly lacks of enough intensity and parallelism, which might lead to missing or wrong information.

Using Göbel mirror and parallel beam optics may solve this problem. Further information can be found in the literature [38].

The incident angles (ω) for investigating the nitrogen implanted layers were 0.5°, 1°, 3° and 5°, and the corresponding effective depths probed by these incident x-ray beams are 38, 76, 228, 380 nm, respectively. Figure 2.3b shows the basic geometry of the GIXRD system.

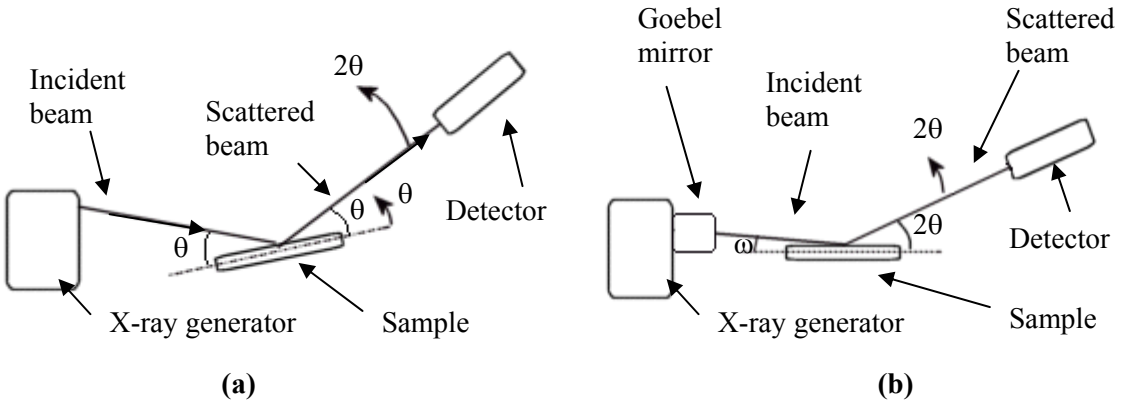

Figure 2.3. Basic geometry of (a) the Bragg-Brentano method and (b) the GIXRD method. Note that the incident beam angle (ω) is fixed during GIXRD analysis and the detector scans 2θ degrees only.

2.3.2 Cross-Sectional SEM Analysis

Cross-sectional SEM analysis performed on selected specimens to examine the possible use of this method for measuring the nitrided and implanted layer thicknesses as well as their surface morphologies.

Before the SEM analysis, the specimens were sectioned and then mounted in the standard bakelite material. Afterwards the specimens were polished down to 0.05 μm alumina solution, and finally etched chemically. The types of chemical etchants were used such that they would preferentially etch the modified layer rather than the substrate. These were 4% nital [100 ml ethanol and 4 ml nitric acid (HNO_3)], Vilella's Reagent [45 ml glycerol, 15 ml nitric acid and 30 ml hydrochloric acid (HCl)] and a special etchant of hydrochloric acid (HCl) and hydrogen peroxide (H_2O_2) with 1:1 volume ratio. Although the etching times were based on the chosen etchant, the typical etching time was from about a few seconds to tens of seconds. Before examining the specimens with either SEM or optical microscopy (OP) all the specimens were cleaned in ethyl alcohol.

Before placing the specimens into the SEM unit, they were cleaned in ethanol and coated by sputter coater which has Au-Pd cathode in order to reduce charging that generally occurs during SEM of metallic samples cast in insulating materials. The typical coating time was about 15 s for plasma ion nitrided specimens and 30 s for nitrogen ion implanted specimens.

Some selected specimens were also analyzed by the SEM in Energy Dispersive X-ray Microanalysis (EDX) mode. The EDX analysis method is based on the detection of x-rays emitted during the interaction of incident electron beam with the material. The emitted x-rays are characteristic to the emitter atoms or the elements. Therefore elemental analysis determination is the main power behind the EDX system.

2.3.3 Optical Microscopy Analysis

The optical microscope (OP) is an important tool for investigating the microstructure of materials, despite the evolution of sophisticated techniques. Optical microscopy analysis can be used to examine the surfaces of as-polished or etched metallographic specimens. In this study optical microscope was mostly used in combination with the differential interference-contrast (DIC) illumination mode. DIC illumination mode produces images with emphasized topographic details similar to those observed using oblique illumination mode [39]. The details that are almost invisible or faintly visible under bright field illumination may be revealed vividly with DIC illumination mode. Besides optical microscopy was also used in combination with SEM analysis. Before the OP analysis, the specimens were prepared in a way similar to those for the SEM analysis [see section 2.3.2].

2.3.4 Mössbauer Analysis

The Mössbauer spectroscopy measurements were made by our collaborator, Prof. Don L. Williamson of Colorado School of Mines, Golden, CO USA. Mössbauer spectroscopy in the backscattering mode provides an excellent technique for studying the types and the concentrations of chemical compounds and metallurgical phases present in these surface layers.

Mössbauer detection methods used in this research involved the backscattering techniques of conversion electron Mössbauer spectroscopy (CEMS) and conversion x-

ray Mössbauer spectroscopy (CXMS). The details with respect to theory of Mössbauer effect, the parameters and the detection techniques can be found in many textbooks and papers [40,41]. So only a brief discussion of the important characteristics for this work will be made.

^{57}Fe CEMS involves the detection of backscattered internal conversion electrons (mainly 7.3 keV from the K-shell), which are emitted with a 90 % probability following the resonant absorption of γ photons (14.4 keV). In the same process, also emitted are the internal conversion x-rays (6.4 keV Kα x-rays) with a 24% probability. The main difference between the two methods lies in their probe depths. The depths are approximately 0.1 μm for CEMS and 12 μm for CXMS [41]. Such a depth analysis is ideally suitable for the examination of typical implantation modified surfaces since the modified layer thicknesses is on the range of 0.1 μm. The CXMS probed depth (~12 μm) is such that it allows us to provide information on the nitrided layer phases extending deeper into the substrate.

Mössbauer spectra were collected at room temperature. A typical Mössbauer analysis result is given as relative emission versus source velocity. Each experimental spectrum was least-square fitted with a superposition of Lorentzian line shapes to yield the spectral parameters: isomer shift (δ in mm/s) (relative to the α-Fe at room temperature), quadrupole splitting (Δ in mm/s), internal magnetic field (H in Tesla) and fractional resonance area (F%). For further details about the analysis refer to the literature [41].

2.4 Mechanical Characterization Techniques

This section involves surface mechanical characterization on the N ion implanted and plasma nitrided layers. These measurements were carried out using the available facilities in Yüzey Teknolojileri Corporation in Çiğli, İzmir.

2.4.1 Roughness Measurements

During ion implantation and plasma nitriding processes material surfaces are subjected to sputtering which might be detrimental to the surface quality of the plastic moulds produced. Thus the sputtering rate of particular treatment may take attention

while preferring specific surface treatment or the parameters used in that treatment. To get an idea about sputtering rates and their effects on the specimens of each process, the specimens were subjected to roughness measurements: roughness profiles and mean roughness values were obtained. Surface roughness measurements were performed on all as-polished, as-plasma nitrided and as-nitrogen ion implanted specimens using a surface profilometer (Mahr). The system probes the surface and the data collection was done automatically with a computer-controlled system. The roughness profiles on selected specimens were plotted by the probed distance versus roughness deviations. The presented roughness values were obtained from five single measurements by averaging.

2.4.2 Nanohardness measurements

Hardness numbers are used primarily as a basis for comparison of materials strengths. In this study to be able to make a quantitative and qualitative comparison between the specimens subjected to different process conditions and treatments, the specimens were subjected to a series of nanohardness measurements. The hardness measurements of as polished, as-nitrided and as-ion implanted specimens were carried out using nanohardness tester (CSEM Instruments) equipped with a Vickers indenter and were evaluated using Oliver & Pharr method. In addition to determination of hardness, the computerized system also measures penetration depth of the indenter based on the indentation. Due to the extremely light load ranges used by the system, which is from 5 mN to 200 mN (0.5 gr to 20 gr), the system is suitable for measuring actual hardness values of quite thin layers. The stage where the specimens are located on during the test is capable of moving in two directions by means of computer controlled servo system and has 0.04 nm resolution in displacement. This characteristic facilitates step-by-step hardness measurements such that one can obtain hardness depth profile (hardness distribution) accurately. Figure 2.4 shows an SEM image of actual hardness measurement (with load of 1 g) distribution impressions of the plasma ion nitrided specimen with nitrogen gas flow ratio of $N_2/H_2 = 1/1$.

When the test starts, the system gradually increases the load up to predetermined load value (determined by the user) denoted by the maximum load (L_{max}) and applies this load in 5 seconds, then the system starts to decrease the load at the same rate. The

loading rate and the unloading rate were determined as follows: loading rate = unloading rate = 2 x (L_{max})/minute.

For example, for a load of 10 mN (1 g), the measurement parameters are given like this: L_{max} = 10 mN and loading rate = unloading rate = 20 mN/minute. As a result 30 seconds requires for both the application and the recovery of the load, which makes 65 seconds indentation time in total, including 5 seconds for the application of L_{max}. The applied load versus time relationship is given in Fig. 2.5.

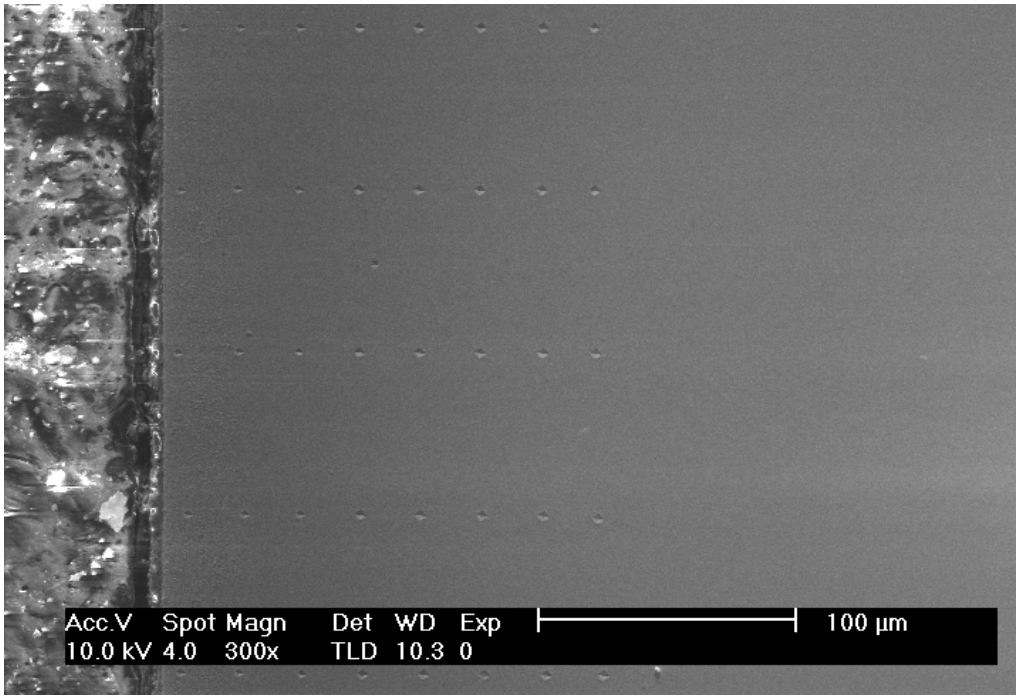

Figure 2.4. SEM image showing an actual hardness measurement (with a load of 1g) distribution impressions of the plasma ion nitrided specimen under nitrogen gas flow ratio of N_2/H_2 = 1/1.

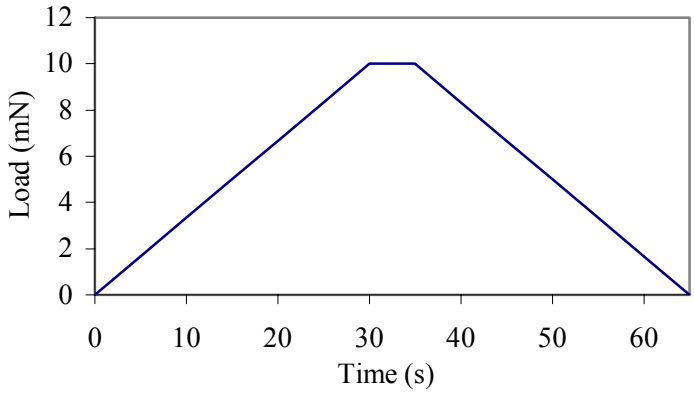

Figure 2.5. An example of load versus time relation during nanohardness measurements with a load of 10 mN (1gr).

Two different types of nanohardness measurements were performed, one of which included nanohardness depth profiling on cross-sections of the as-plasma nitrided and as-implanted specimens and the other included hardness measurements on the surfaces of the nitrogen implanted specimens. The latter measurement gives the surface hardness value while the previous gives the hardness depth distribution for the tested specimens.

2.4.2.1 Nanohardness Depth Profiling

Selected specimens were sectioned, bakelited and then polished to mirror like quality. Then to provide cross-sectional hardness distribution of the samples, a series of measurements were carried out step by step from the inner surface (the substrate side) to the outer surface (the nitrided or ion implanted side), on the cross-section of the samples.

Five indentations were made at a given depth horizontally. The number of measurement steps which would be made vertically was determined separately for each sample by doing pre-test. One important feature here was that the distance between each indentation made vertically along the nitrided layer was at least five times bigger than the dimensions of the trace modified plastically by the tip of the indenter. On the other hand this distance should also be as short as possible to be able to obtain a meaningful data for hardness depth profiling. For example, the thickness of the indentation trace was about 1 μm when the applied load of 0.5 g was used. Therefore, the distance between each indentation made vertically and horizontally along the nitrided layers were chosen as 6 μm and 25 μm, respectively. The loads chosen for the nanohardness

measurements were 10 mN (1g), and 5 mN (0.5g), for the nitrided and ion implanted specimens, respectively.

2.4.2.3 Surface Hardness Measurements

The surface hardness profiles of the as-polished and the nitrogen ion implanted specimens were obtained as a function of the indenter load. The loads and the corresponding Vickers numbers were 0.5 g (HV 0.005), 1 g (HV 0.01), 2.5 g (HV 0.025), 5 g (HV 0.05), 10 g (HV 0.1), and 20 g (HV 0.2). The hardness values on the surfaces of the nitrided specimens were not measured due to the increased surface roughness (the RMS roughness for the N_2/H_2 =3/1 sample specimen is about 0.84 μm whereas the RMS roughness of the as-polished specimen is 0.02 μm).

2.4.3 Friction and Wear Analyses

Tribological testing was accomplished on selected specimens using a ball-on-disc wear tester (CSEM Instruments, high temperature tribometer) under dry cyclic sliding motion. During the measurements, Al_2O_3 was used as a counter body. The tribo testing involved as-polished, as-nitrided, as-nitrogen ion implanted disc specimens with 3.00 cm in diameter and 4.00 mm in thickness rotated radially at a predetermined speed, while the alumina ball, 6.00 mm in diameter, has a contact with the surface of the specimen. The predetermined normal load is applied to the specimen and induces wear during the operation. Under these conditions, the ball induces wear tracks circumferentially around the disc at predetermined radius that was chosen to be 7 mm. The contact load was chosen as 1 N (100 g) for all the tribological testings, yielding a contact pressure of roughly 100 MPa [42]. Assuming that each rotation of the testing sample under wear mode corresponds to the cyclic load of the plastic injection mould, the measurement then can be carried out based on the number of laps of the rotational motion. The number of laps therefore was chosen to be 5000 to in and out compensate a typical loading number of the plastic injection mould. During all the measurements no lubricant was used (i.e. dry sliding) and the measurements were carried out under pure nitrogen (N_2 %99.99) atmosphere. The humidity of the system was measured with a hygrometer and was found to be about 50 % during all the measurements. During the testing the computer-controlled machine yields the friction coefficient values. When the

test is completed quantitative wear results are obtained by using surface profilometer. Probing the wear track by the profilometer, the area of the wear tracks as well as the wear profiles are obtained. The presented wear track areas are given in averaging and the friction coefficient values were plotted against the number of laps.

A schematic representation of the oscillating ball-on-disc (or pin-on-disc) tribo system is shown in Fig. 2.6. The tribological testing parameters given in Table 2.4 were constant for all the measurements.

Table 2.4. Tribo test parameters used for wear and friction analyses of plasma nitrided and nitrogen implanted specimens

Applied load (N)	Number of rotations	Distance (m)	Sliding wear speed (cm/s)	Atmosphere	Temperature (°C)
1	5000	220	5	Pure N_2 (%99.99)	22-24

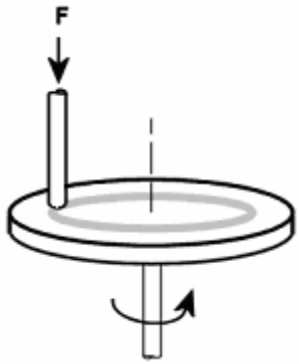

Figure 2.6. A schematic representation of the oscillating pin-on-disc tribo tester.

2.4.4 Corrosion Analysis

Corrosion analysis measurements were done at Dönmez Debriyaj Corporation in Çiğli, İzmir. The corrosion analysis system, whose schematic drawing is shown in Fig. 2.7, is used to simulate and control the conditions of corrosive environments and the analysis results are important in terms of relative change in the corrosion behaviour and the corrosion initiation duration. The analysis involved in subjecting selected as-polished, as-plasma ion nitrided and as-nitrogen ion implanted samples to a dispersed mist, consisting of 2% salt (NaCl) solution in distilled water (ASTM B117). The mist is

produced by means of mist dispersion tower. The main function of the tower is to spray the salt solution over the specimens.

In this system, the specimens are fixed to the sample holders in a slightly inclined position and placed into the reaction chamber. The reason for placing the specimens in an inclined position is to prevent the surface of the samples from salt precipitation. After filling the tank with the salt solution, the pump starts running to spray the salt solution over the specimens. During the analysis, the specimens are regularly checked by means of transparent top cover of the reaction chamber whether any corrosion initiation occurs or not. When the corrosion initiation is observed, the test is stopped to take the corroded specimen out. After noting the duration for the corrosion initiation, the system is started to run again for the other test specimens. One important feature of the measurement was that the analysis duration is restricted to the working hours of the company. This restriction was resulted in stopping the test before the corrosion initiation observation accomplished for one of the specimens. However, this drawback was not resulted in loss of important data. After the corrosion testing, the digital photographs were also taken from the surfaces of all the test specimens.

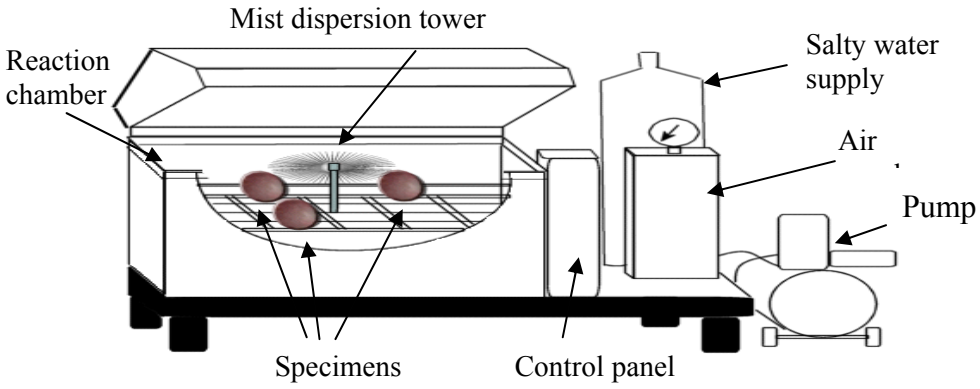

Figure 2.7. A schematic representation of the salt spray analysis system.

CHAPTER 3

NITRIDING AND IMPLANTATION INDUCED PHASES

3.1 Plasma Nitriding Induced Phases

3.1.1 XRD Results

In this section microstructures produced as a result of plasma ion nitriding and nitrogen ion implantation will be considered. Figure 3.1 shows the XRD results for the nitrided specimens with the gas composition ratios of N_2/H_2 = 1/10, 1/1, and 3/1 corresponding to the nitrided samples SC11, SC4, and SC14 (see Table 2.2). Included in the same figure are the results for the as-polished sample (the substrate material).

In Fig. 3.1, the substrate (X36CrMo17) peaks are labelled as bcc α-(Fe,Cr,Mn) phase and as "C". The latter refers to the CrFe-carbide phase ($Cr_{\sim 16}Fe_{\sim 7}C_6$) and its volume percent is estimated to be about 2 to 3 % based on the integrated intensity calculations of the XRD peaks. Note that the square-root of the intensity is plotted to reveal more clearly the weaker peaks.

The plasma nitriding induced peaks associated with the various crystal structures represented in Fig. 3.1 are labelled with appropriate Miller indices as well. Note that the data shown in the figure are progressively offset for clarity. Important key features made on the process of identifying the present phases in the treated specimens is such that (1) ε-(Fe_3N) has distinct peaks at 39 and 58 degrees, (2) CrN has a distinct peak at 38 degree, and (3) γ′-(Fe_4N) has a distinct peak at 48 degree in 2θ, which show no overlap with any other peaks of the phases. These features which are also supported by the literature [16,28,43,44] allowed us to make accurate phase identification and clear the picture of the regions where overlapping occurs.

The XRD results for the plasma nitrided specimens with various N_2+H_2 gas compositions clearly show the formation of (Fe,Cr,Mn)-nitrides, and CrN in the top nitrided layers. The (Fe,Cr,Mn)-nitrides are of the following type: (1) ε-Fe_3N with both

paramagnetic and magnetic characteristics [23,27], and (2) γ'-Fe_4N. Here we have ε-$(Fe,Cr,Mn)_{2+x}N$ with x~1 and γ'-$(Fe,Cr,Mn)_4N$.

While the formation of CrN is observed for all the nitriding conditions, the ε-(Fe_3N) and γ'-(Fe_4N) nitrides, are only formed for higher gas flow rate samples (N_2/H_2=1/1 and 3/1 specimens, see Table 2.2). The clear observation of CrN under the nitriding temperatures of this study (520-540 ^oC) regardless of the various gas mixtures of N_2+H_2 is consistent with earlier studies [9,22], which show that CrN begins to precipitate when plasma nitriding high-chromium steels at temperatures above 450 ^oC. This compositional phase segregation adversely affects the corrosion resistance of the treated steel and the compound layer since it spoils the passivated chromium component out of its homogeneous distribution in steel leaving the Cr-depleted matrix unprotected [20,22,45].

In our case, the dissolution of the Cr results in a phase separated mixture of bcc-Fe(Mn) and CrN. As a result of plasma nitriding, the intensities of the substrate XRD peaks is seen to be reduced due to increasing nitrided layer thickness. Semi quantitative and qualitative analyses of the XRD data in Fig. 3.1 indicate that the N_2/H_2=1/1 specimen has much higher amounts of ε-(Fe_3N) and γ'-(Fe_4N) nitrides in the top nitrided layer (compound layer) in comparison to the sample with the N_2/H_2=3/1 which shows weak XRD peaks for these phases. The lower contents for these phases for the latter N rich conditions might be due to the intense sputtering taking place during plasma nitriding at high gas composition ratios (the rms roughness for the specimen nitrided under the N_2/H_2=3/1 plasma processing conditions is ~ 0.84 μm in comparison to those for the N_2/H_2=1/1 and the as-polished specimens, which are ~ 0.40 μm, and 0.02 μm, respectively).

Following the observation of Cr depletion, the lattice constant analysis associated with the substrate peaks reveals some interesting features. The lattice parameter (a_o) of the substrate material phase α-(Fe,Cr,Mn) was calculated to be 2.8745 Å by the method of least squares (extrapolating the measured lattice parameters against $\sin^2\theta$ based on the XRD peaks.) (The detailed explanations about this method could be found in the textbook, Elements of X-ray Diffraction.) Therefore we can make a comment that substitution of Cr and Mn results in a slightly larger lattice constant in

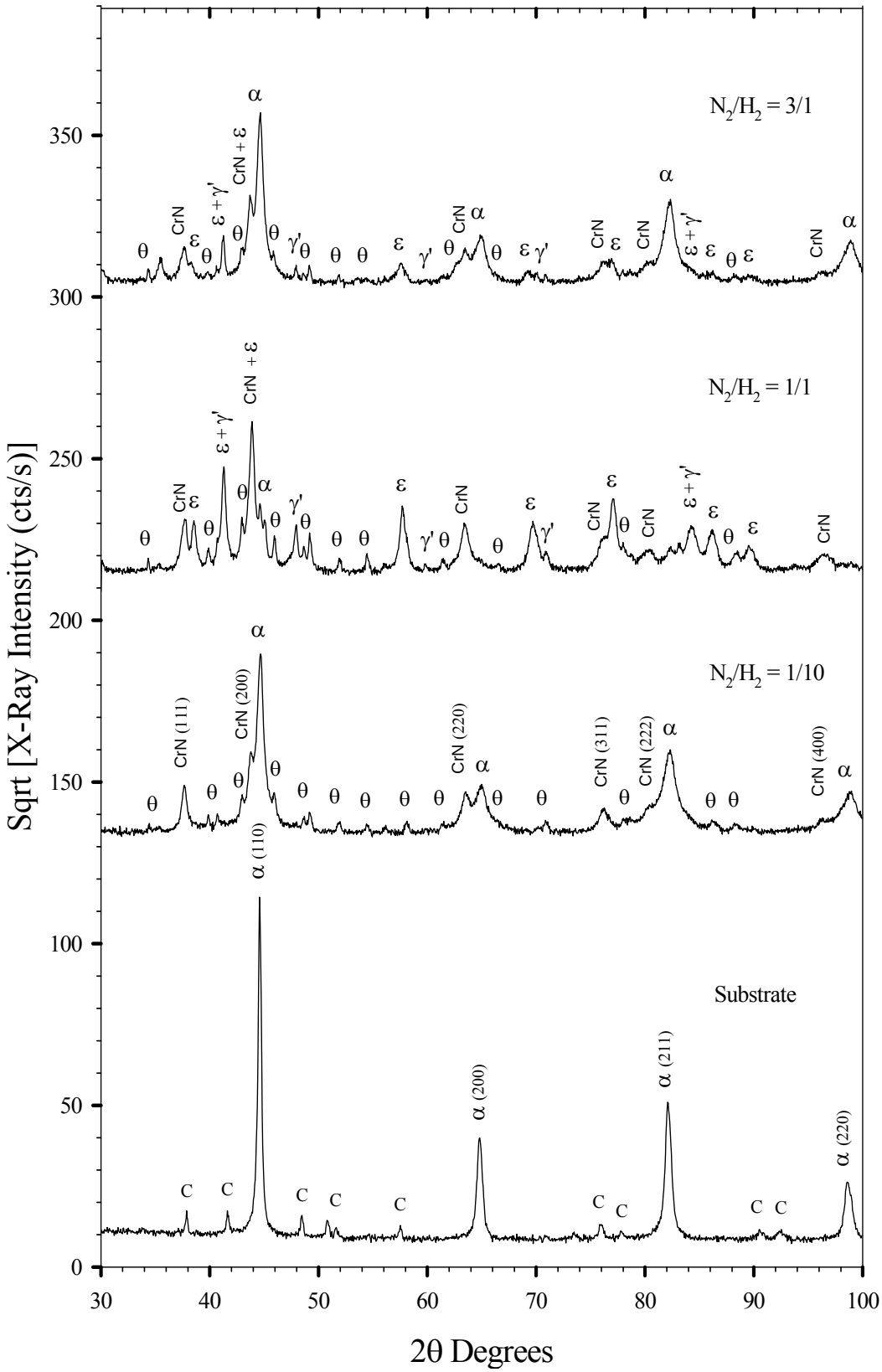

Figure 3.1. XRD patterns of as-polished (the substrate) and the plasma ion nitrided specimens under N_2/H_2 =1/10, 1/1, and 3/1 gas flow ratios. The peaks associated with the various crystal structures are labelled.

comparison to that of the pure iron, because according to the literature [46], the lattice parameter of pure bcc iron, α-Fe is 2.8665 Å. The same procedure is followed for the ion-nitrided and nitrogen ion implanted specimens and the results are presented in Table 3.1. The observed shifts in the α-(Fe,Cr,Mn) lattice parameters for the nitrided specimens reveal that the depletion of Cr from the lattice leaves the lattice much like pure α-Fe. These results are consistent with those obtained from both CEMS and CXMS (to be discussed in the next section).

Table 3.1. The calculated lattice parameters for the plasma ion nitrided and N ion implanted specimens.

Pure Iron	2.8665 Å	Observed change in Lattice Constant
α-(Fe,Cr,Mn)	2.8745	
Plasma Nitrided Specimens		
SC10, SC11, SC12	2.8693	Decrease
SC3, SC4, SC5, SC6*	-	-
SC13, SC14, SC15	2.8711	Decrease
N Ion Implanted specimens		
SC7, SC8, SC9	2.8756	Increase
SC10, SC11, SC12	2.8796	Increase

* The lattice parameter of these specimens could not be evaluated due to the low substrate peak intensities and the overlap of the substrate peaks with those of the other peaks.

The XRD data also shows the existence of small intensity peaks labelled θ in Figure 3.1. These peaks are identified as those of cementite, Fe_3C [JCPDS database (PDF # 35-0772)]. There may also be some Mn and Cr substitution in this phase [i.e $(Fe,Cr,Mn)_3C$]. Both CEMS and CXMS results (to be discussed in the next section) are also consistent with the observation of Fe_3C-like phase. It appears that the CrFe-carbide phase ($Cr_{\sim 16}Fe_{\sim 7}C_6$) has converted into cementite. This finding raises some important questions regarding the nitriding process, and will be discussed in the next section.

3.1.2 Mössbauer Results

Figures 3.2, 3.3, 3.4 3.5 and Table 3.2 show the CEMS and CXMS results for the as-polished specimen and the plasma nitrided specimens with the N_2+H_2 gas composition ratios of 1/10, 1/1, and 3/1 (corresponding to SC11, SC4, and SC14,

respectively). The CEMS and CXMS spectra of the as-polished sample are composed of magnetic, bcc α-(Fe,Cr,Mn), and paramagnetic components (denoted as SS1, SS2, and SS3 in Table 3.2). The magnetic subspectra (H = 31.0 T and H = 26.9 T) are consistent with Fe-Cr alloys with a wide range of nearest neighbour environments around the resonant Fe. The small paramagnetic component (SS3) in Figure 3.2 is attributed to Fe in the CrFe-carbide phase and this is consistent with the XRD results. The CEMS and CXMS regions are similar.

Table 3.2. The Mössbauer spectral fit parameters associated with the as polished and plasma nitrided specimens. Note that the spectral parameters in this table δ, Δ, H and F correspond to isomer shift, quadrupole splitting, internal magnetic field and fractional resonance area, respectively. "f" in parentheses indicates that the parameter was fixed.

Sample SS#	**CXMS**				**CEMS**			
As-pol.	δ (mm/s)	Δ (mm/s)	H (T)	F (%)	δ (mm/s)	Δ (mm/s)	H (T)	F (%)
SS1	+0.01	+0.02	31.1	59	+0.01	+0.02	31.0	61
SS2	-0.05	-0.03	27.1	39	-0.04	+0.03	26.9	36
SS3	+0.04	0	0	2	+0.04	0	0	3
SC11 (1/10)								
SS1	+0.01	0.00	33.19	66	+0.01	0.00	33.13	70
SS2	-0.03	+0.04	30.29	29	-	-	-	0
SS3	+0.22	+0.05(f)	20.6	5	+0.19	+0.05	20.5	30
SC4 (1/1)								
SS1	+0.29	-0.02	23.7	53	+0.30	0.00	23.6	69
SS2	+0.18	+0.03	20.8	23	+0.19	+0.03	20.7	22
SS3	+0.01	0(f)	33.14	24	0(f)	0(f)	33.0	9
SC14 (3/1)								
SS1	+0.01	+0.01	33.11	79	+0.01	0(f)	33.19	35
SS2	+0.33	0.00	23.6	21	+0.34	0.00	23.62	48
SS3	-	-	-	0	+0.39	0.87	0	17

The CEMS results of the plasma nitrided specimen SC11 under N_2/H_2= 1/10 gas flow ratio conditions shows the nearly complete decomposition of the pure surface layer [α-(Fe,Cr,Mn)] into relatively pure bcc Fe[α-Fe(Mn)] [H = 33.13 T, F = 70 %, Table 3.2] and a magnetic phase whose Mössbauer parameters are quite similar with those of cementite, θ-Fe_3C (H = 20.7-20.8 T and IS = 0.18 mm/s, Table 3.2). CXMS, probing

much deeper (~ 12 μm), shows some of the original α-(Fe,Cr,Mn) alloy (the substrate phase) (H = 30.9 T), however this region is also highly decomposed. It is assumed that some Cr that is depleted from the FeCr-alloy is also forming CrN based on the XRD results for the specimen nitrided under the N_2/H_2 = 1/10 conditions. The large CEMS $(Fe,Cr,Mn)_3C$-like resonance fraction (30%) suggests significant carbon segregation to the near-surface region. This finding raises some important questions regarding the nitriding process, and is discussed later.

The Mössbauer results for the specimen nitrided under the N_2/H_2=1/1 conditions show the strongest resonance signals of the three specimens investigated. The CEMS data shows two distinct magnetic signals, one of which (H = 20.7 T, see Table 3.2) is cementite-like [$(Fe,Cr,Mn)_3C$] and is the same as found for the N_2/H_2 = 1/10 sample, and the other is associated with an (Fe,Cr,Mn)-nitride whose Mössbauer parameters (H = 23.6-23.7 T, see Table 3.2) are similar to those of ε-$Fe_{3.2}N$ [47]. Here, we have ε-$(Fe,Cr,Mn)_{2+x}N$ with x ~ 1. The CXMS results show that a significant amount of the ε-nitride phase is found to be distributed deeper into the nitrided layer. The CEMS and CXMS findings of the ε-nitride phase are quite consistent with the strong ε-nitride XRD signals.

The CEMS results for the higher gas flow ratio conditions (N_2/H_2=3/1) show a strong ε-nitride signal near the surface of the nitrided layer (~ 0.1 μm). The CXMS results indicate that the nitride signal gets much weaker as one probes deeper into the nitrided layer. However, the CXMS results also show that significant amount of decomposition (into pure α-Fe(Mn) + CrN + ε-nitride) occurring deeper into the substrate. Both CEMS and CXMS findings of the ε-nitride phase agrees quite well with those of the XRD results (the XRD ε-phase peaks for the N_2/H_2=3/1 sample are much weaker in comparison with those of the N_2/H_2=1/1 sample). The CEMS results for the N_2/H_2=3/1 sample, in addition to magnetic ε-nitride signal, shows a paramagnetic component which suggests a higher content N phase. However, the Mössbauer parameters for this doublet (QS=0.87 mm/s, see Table 2) does not match those expected for Fe_2N [10]. The CEMS results for the N_2/H_2=3/1 nitriding conditions shows the disappearance of the Fe_3C-like resonance with H = 20.5-20.8 T (see Table 3.2) that was

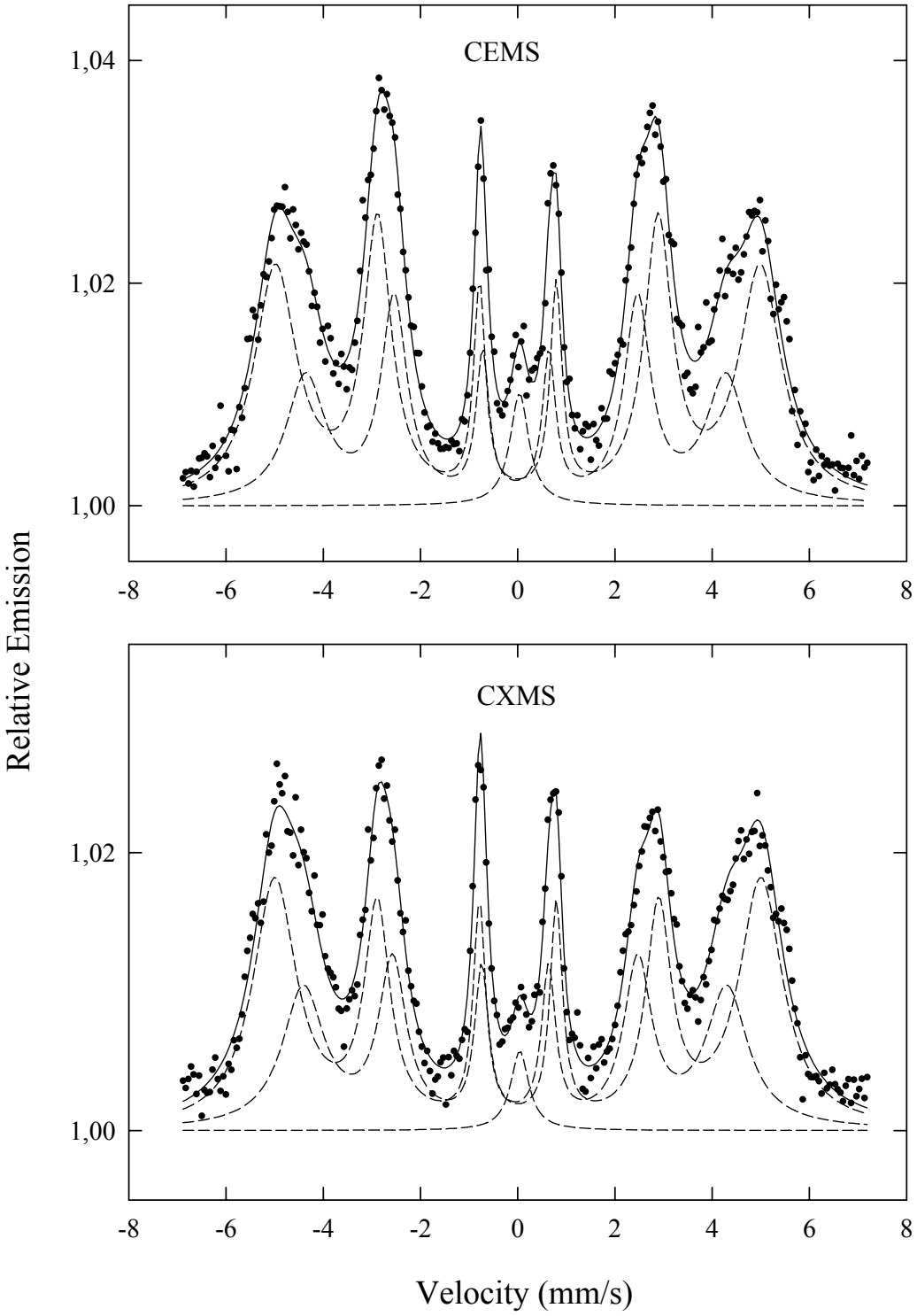

Figure 3.2. CEMS and CXMS data and the computer fits for the substrate material. The dashed lines are the fitted sub spectra to the Mössbauer spectrum.

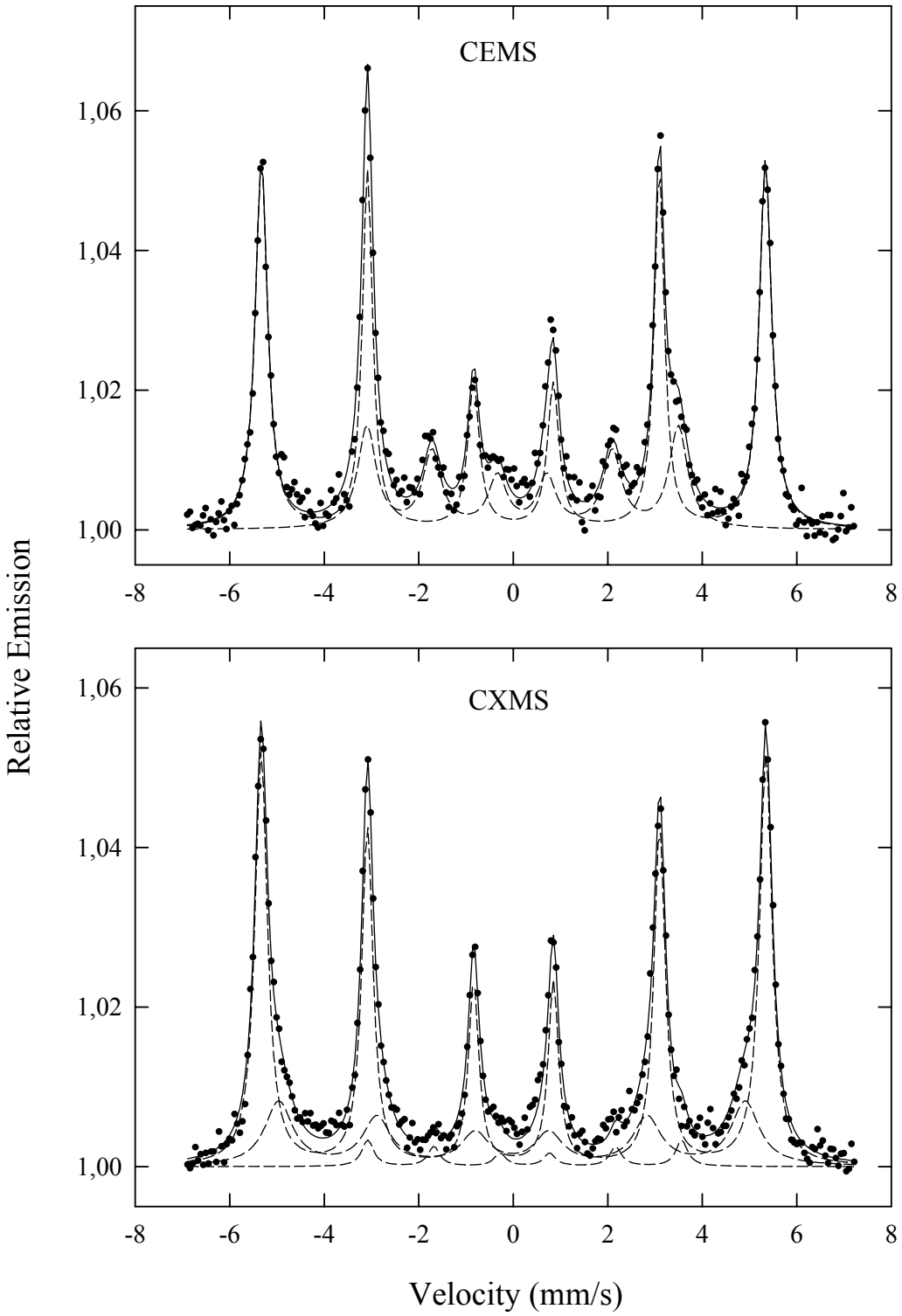

Figure 3.3. CEMS and CXMS data and the computer fits for the plasma nitrided specimen SC11 under the N_2/H_2 =1/10 conditions.

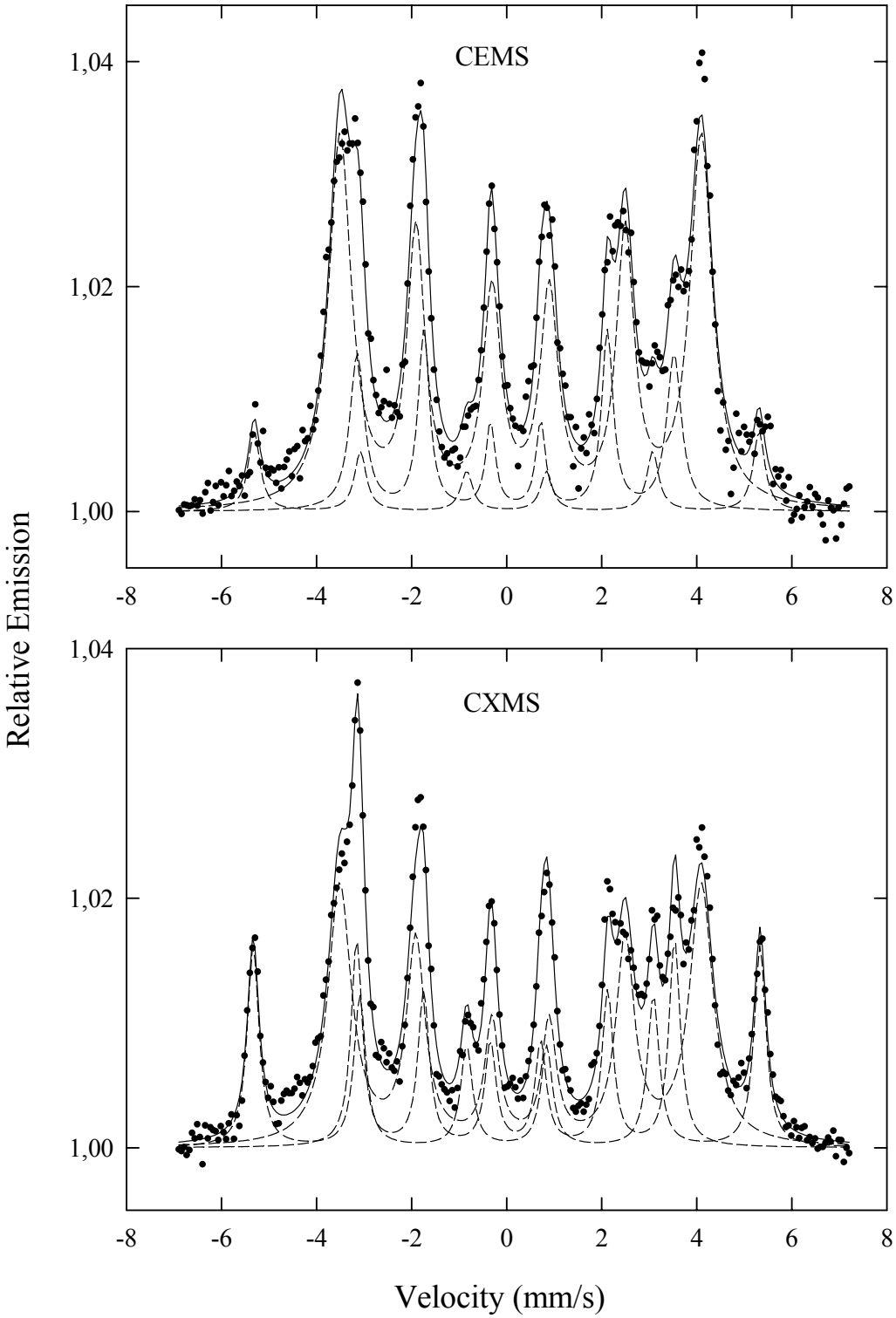

Figure 3.4. CEMS and CXMS data and computer fits for the plasma nitrided specimen SC4 under the N_2/H_2 =1/1 conditions.

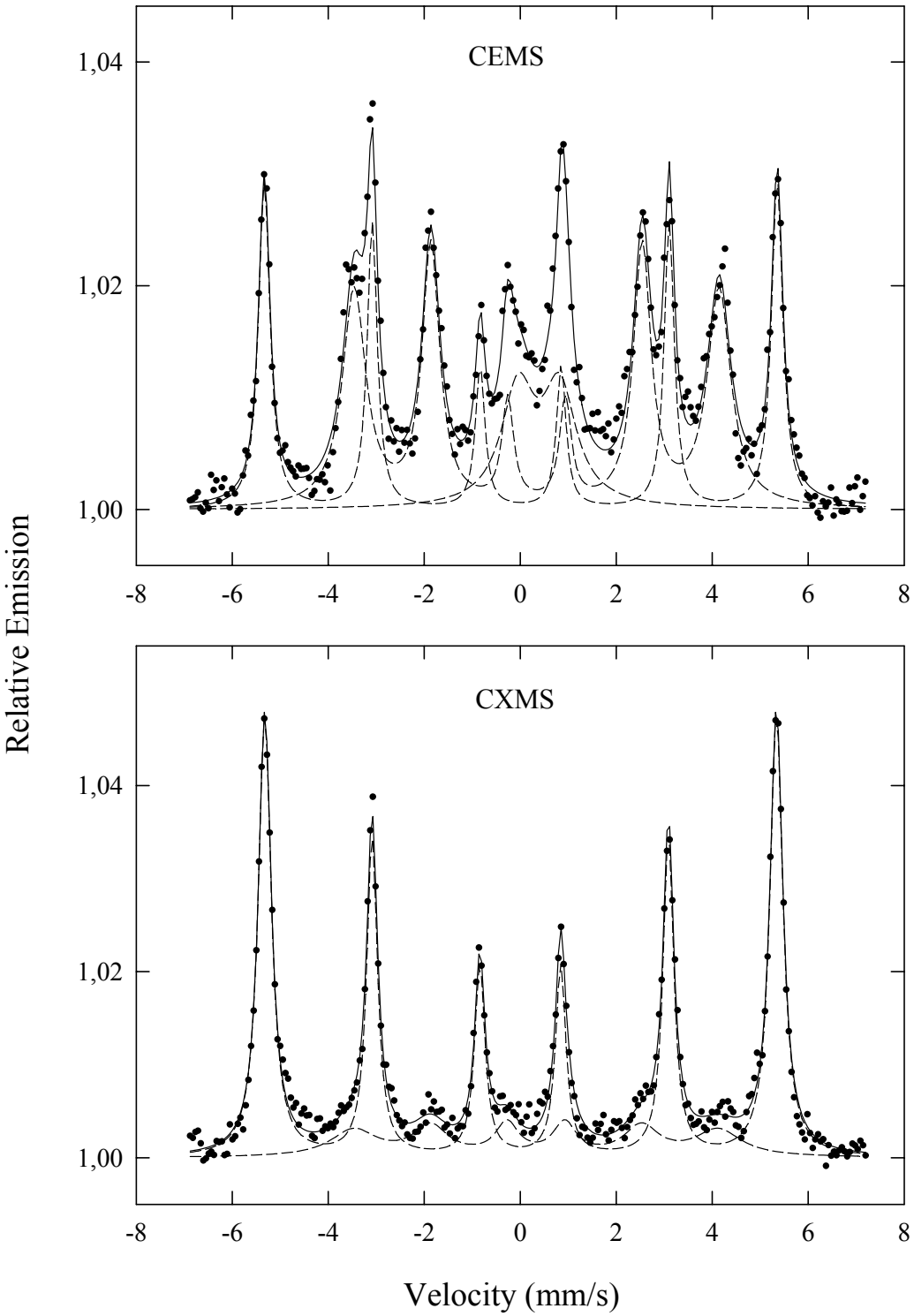

Figure 3.5. CEMS and CXMS data and the computer fits for the plasma nitrided specimen SC14 under the N_2/H_2 =3/1 conditions.

significantly present for the N_2/H_2=1/10 and 1/1 samples. Perhaps the cementite-like resonance has somehow converted into the paramagnetic phase as something like $(FeMn)_3(CN)$, still having the Fe_3C-like crystal structure but now with paramagnetic characteristics.

The Mössbauer resonance fractions associated with the Fe_3C-like phase, $[(Fe,Cr,Mn)_3C]$, raises some questions and merits further discussion. This fraction is 5% based on the CXMS resonance and it is 30% based on that of the CEMS. The 5% CXMS fraction seems reasonable assuming the CrFe-carbide phase, $Cr_{\sim 16}Fe_{\sim 7}C_6$, has converted into cementite (Fe_3C) and that all the carbon from the carbide is used to form the cementite (the 2% CXMS resonance signal in the as-polished state should increase to about 5% in the N_2/H_2=1/10 sample). On the other hand, the much larger CEMS resonance fraction (30%) seems difficult to explain unless there is some carbon segregation taking place near the surface region. We believe that the larger fraction is due to the extra carbon in the nitriding chamber since plastic injection mould materials to be nitrided along with our specimens probably were not cleaned carefully and had some oil residues on them before the nitriding step. The extra carbon may also be entering the nitriding system via the diffusion pump. Note that the CEMS and CXMS cementite-like resonance fractions for the N_2/H_2=1/1 sample are about the same (~ 23%), and the 23% CXMS fraction may be interpreted as the conversion of the CrFe-carbide phase into the cementite-like phase deeper in the substrate assuming the extra C is supplied by the mechanism(s) just mentioned.

Also, the clear observation of γ'-Fe_4N nitride by XRD for the specimens nitrided under the N_2/H_2=1/1, and 3/1 nitriding conditions (Fig. 1) but not by CEMS can be explained by the fact that the presence of any γ'-nitride in the Mössbauer may be masked by the ε-nitride, Fe_3C-like carbide, and α-Fe(Mn) signals.

3.2 Implantation Induced Phases

3.2.1 XRD Results

The grazing incidence x-ray diffraction (GIXRD) results at the incident angles of 0.5, 1, 3, and 5 degrees for the specimens nitrogen ion implanted to doses of $2x10^{17}$ and $1x10^{18}$ ions/cm^2 are shown in Figs. 3.6 and 3.7, respectively. The top data in these figures were obtained by the symmetric θ-2θ (Bragg-Brentano) mode. Note that these

spectra shown in these figures progressively offset for clarity. The effective depths (<x> ~ sinω/μ) probed by these fixed x-ray beams incident on the samples are about 38 nm, 76 nm, 228 nm, and 380 nm corresponding to the incident angles of 0.5, 1, 3, and 5 degrees. These numbers are based on the linear mass absorption coefficient for the bulk material (0.23 μm^{-1}).

The top (θ-2θ) scan peaks labelled as α(hkl) and C in Figs 3.6 and 3.7 refer to the substrate phases of α-(Fe,Cr,Mn) phase and the CrFe-carbide phase ($Cr_{\sim 16}Fe_{\sim 7}C_6$) (see section 3.1.1). The GIXRD scan at the lowest angle (0.5°) in Fig. 3.6 indicates that the top N ion implanted layer (~38 nm) is composed of the hexagonal nitride phase ε-$(Fe,Cr,Mn)_{2+x}N$ with compositions x changing from 0-1 suggested by the broad XRD peaks [30]. As the incident angles increases more contribution from the substrate is observed. The GIXRD results at 1° shows significant amount of ε-phase is distributed within the top N implanted layer (~76 nm). The GIXRD results at higher incident angles (3° and 5°) show more and more contribution coming from the substrate phase (the relative intensities of substrate α-(Fe,Cr,Mn) peaks compared to the ε-phase peaks increases) due to the increased penetration depths at these angles.

Similar to the lower dose nitrogen ion implanted specimen, the top surface layer of the higher dose implanted specimen (Fig. 3.7) is also found to be composed of the hexagonal nitride phase ε-$(Fe,Cr,Mn)_{2+x}N$ extending up to about 40 nm (at 1˚) with compositions x changing from 0-1 indicated by the broad XRD peaks.

A qualitative comparison made between the lower dose $2x10^{17}$ ions/cm^2 and the higher dose $1x10^{18}$ ions/cm^2 N implanted specimens suggests thicker and N content richer ε-phase for the higher dose N implanted sample. This comparison is based on the broadness and relative intensities of the ε-phase peaks in Figs. 3.6 and 3.7. However, the sharper ε-nitride peaks observed for the lower dose implanted specimen suggests that the crystallinity of ε-nitride phase is better for this sample compared to the higher dose implanted specimen.

Another observation based on the XRD results in Fig.3.7 shows that the strongly broadened ε-$(Fe,Cr,Mn)_{2+x}N$ peaks show an asymmetry toward higher diffraction angles, suggesting a nonuniform nitrogen distribution or concentration gradient in the implanted layer, particularly for the high dose N implanted sample. This concentration

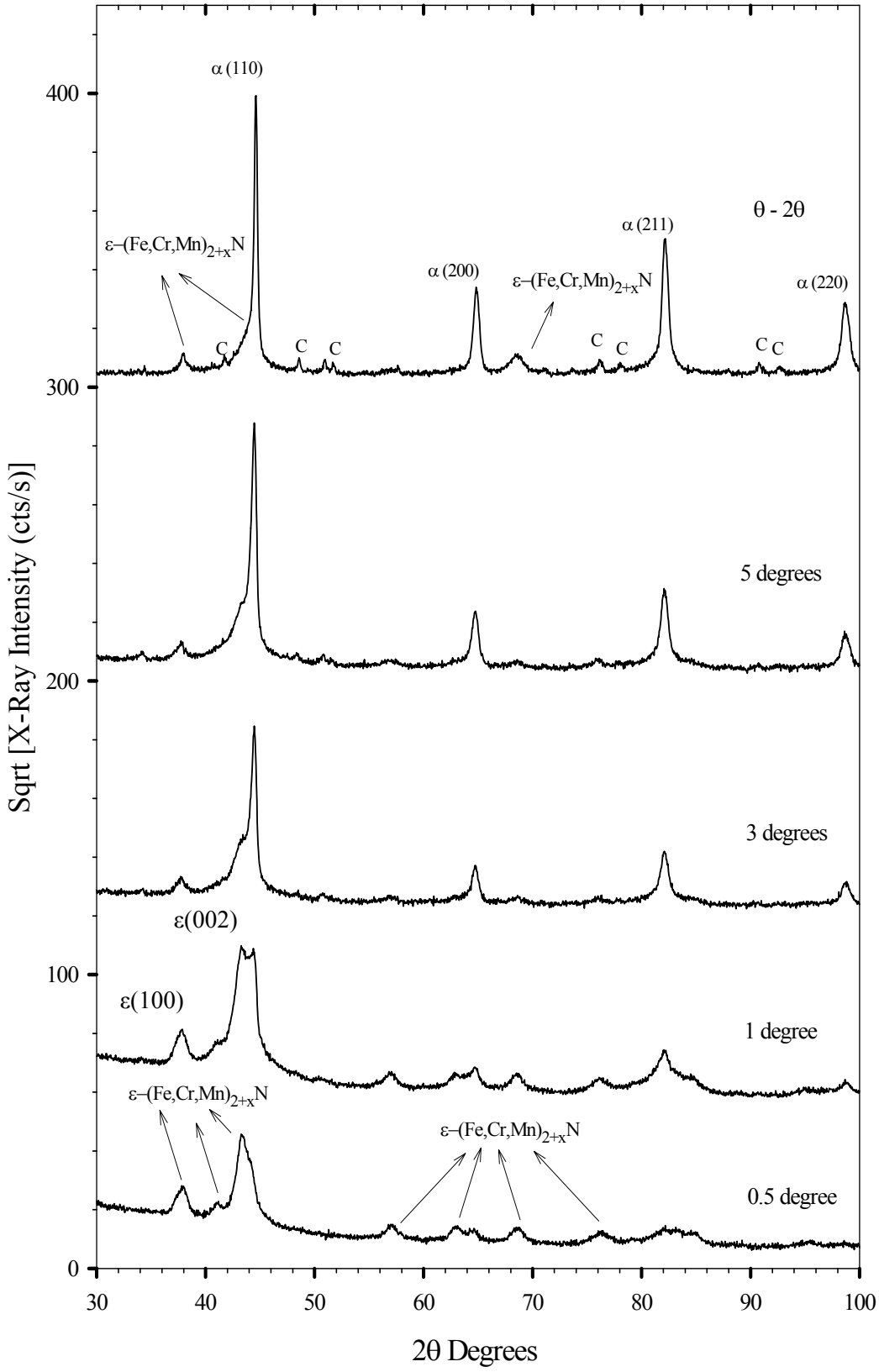

Figure 3.6. GIXRD patterns for the low dose ($2x10^{17}$ ions/cm^2) nitrogen implanted specimen. Note that the top scan in this figure is the normal θ-2θ (Bragg-Brentano) method.

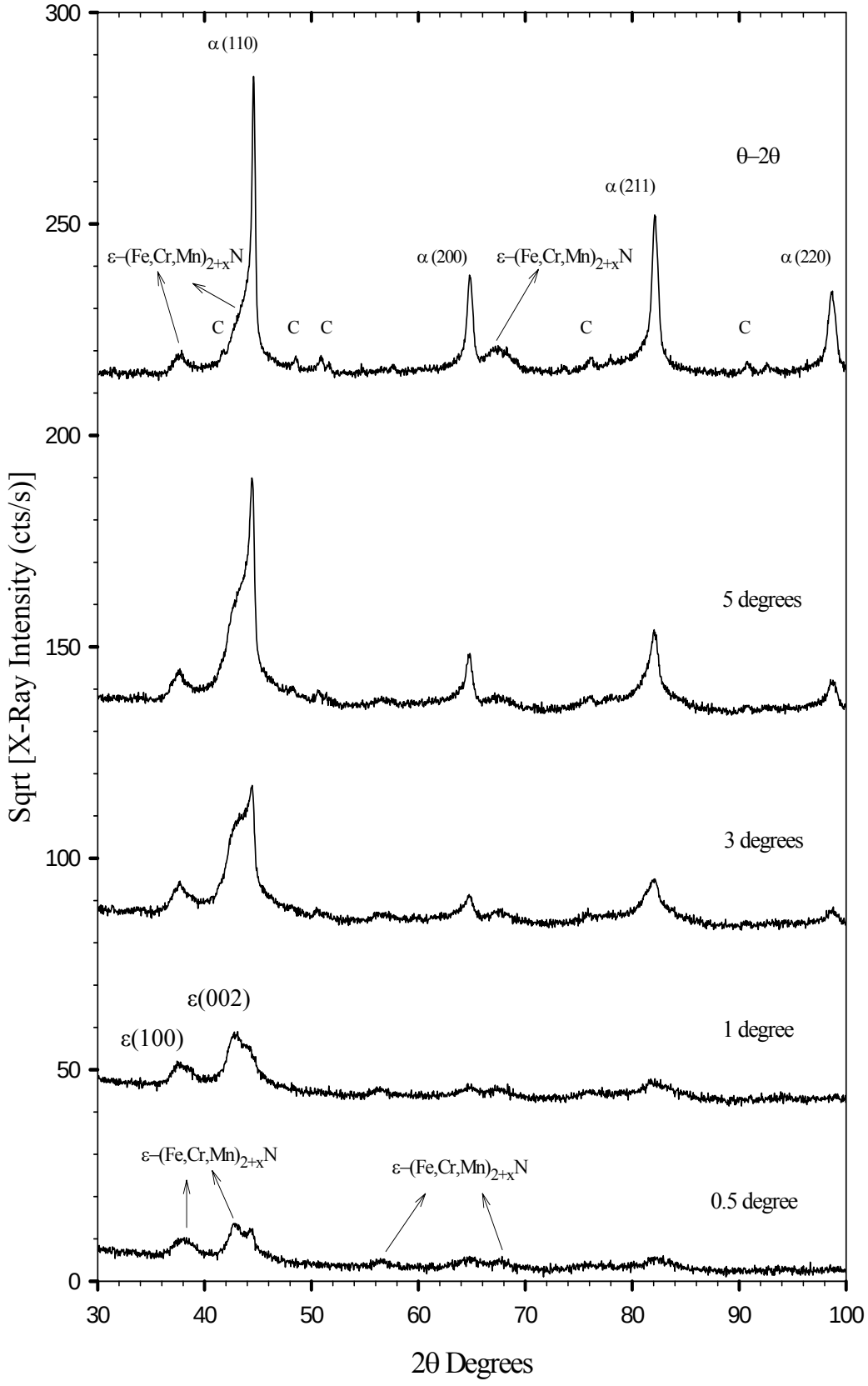

Figure 3.7. GIXRD patterns for the high dose ($1x10^{18}$ ions/cm^2) nitrogen implanted specimen. Note that the top scan in this figure is the normal θ-2θ (Bragg-Brentano) method.

gradient should induce lattice distortion. The calculated lattice parameters for the substrate phase [α-(Fe,Cr,Mn)] for the N ion implanted samples listed in Table 3.1, also indicate free nitrogen in the bcc lattice and agree quite well with this observation. Note that the substrate peaks in Figs. 3.6 and 3.7 are slightly shifted to lower angles. This result also indicates that the N implanted layers are under some compressive stresses. This might be attributed to the insertion of interstitial solid solution atoms as well as the formation of precipitates. The interstices in the metal-atom arrangements of iron are two types, surrounded respectively by a tetrahedron of four metal atoms and by an octahedron of six metal atoms. Nitrogen always occupies the octahedral holes in all three metal structures and never the tetrahedral ones. The insertion of interstitial nitrogen restores the regular metal-atom environment but produces a large anisotropic strain in the surrounding matrix [12].

3.2.2 Mössbauer Results

The CEMS results of the nitrogen ion implanted specimens are shown in Fig. 3.8 and the spectral parameters obtained by computer fitting are given in Table 3.3. Note that the data for the low dose N implanted specimen were rather complex and some of the parameters had to be fixed (f) at the values obtained from the as-polished sample.

Table 3.3. CEMS spectral parameters obtained by computer fitting for the N ion implanted specimens at $2x10^{17}$ and $1x10^{18}$ ions/cm^2 doses.

Sample	SS#	δ (mm/s)	Δ (mm/s)	H (T)	F (%)
SC7 ($2x10^{17}$)	SS1	+0.01(f)	+0.02(f)	31.0(f)	45
	SS2	-0.04(f)	-0.03(f)	26.9(f)	12
	SS3	+0.1	0	0	2
	SS4	+0.035(f)	0(f)	19.6	23
	SS5	+0.41(f)	0(f)	6.9	18
SC18 ($1x10^{18}$)	SS1	+0.01(f)	+0.02(f)	31.0	30
	SS2	-0.04(f)	-0.03(f)	27.2	8
	SS3	+0.40	0.37	0	46
	SS4	+0.26	0(f)	20.2	16

The CEMS spectra of the low dose implanted ($2x10^{17}$ ions/cm^2) sample is composed of magnetic substrate phase [bcc α-(Fe,Cr,Mn)] and magnetic phases whose

Mössbauer parameters are quite similar to those of ε-$Fe_{2.67}N$ - $Fe_{2.47}N$ reported in the literature [48]. Here we must have ε-$(Fe,Cr,Mn)_{2.67}N$ and $(Fe,Cr,Mn)_{2.47}N$.

The CEMS spectra for the high dose ($1x10^{18}$ ions/cm^2) N implanted specimen (SC18) is also shown in Fig. 3.8, and consists of magnetic and paramagnetic components. The magnetic component (H=20.2 T, Table 3.3) is also attributed to ε-$(Fe,Cr,Mn)_{2+x}N$ with x values similar to those for the low dose implanted sample and to those in the literature [48]. The strong paramagnetic component in the high dose N implanted specimen is quite consistent with an Fe_2N-like phase (here, of course we must have ε-$(Fe,Cr,Mn)_{2+x}N$ with x~0, however, the quadrupole splitting parameter (Δ for SS3, Table 3.3) is somewhat larger than the 0.26-0.29 mm/s values reported for ε-Fe_2N in the literature [48].

The quantitative CEMS results in Table 3.3 suggests richer N content for the high dose N implanted specimen (SC18) compared to the low dose N implanted sample (SC7). The total resonance fractions of nitrides in SC7 (F = 43%) and SC18 (F = 62%) corresponds to the surface layer thickness of about 40 nm and 65 nm, respectively, based on a uniform layer of nitride phase assumption [49]. If, however, the phases are distributed within the substrate, and therefore not a uniform layer of nitride, the nitrided layer could be thicker. The nitrogen implanted layer thicknesses obtained from the CEMS fractions of nitrides (based on a uniform layer of ε-nitride assumption) also agree quite reasonably with the ballistic depth range for the 85 keV N ions based on TRIM [50] calculations. This range for 85 keV N ions is estimated to be ~ 90 nm.

The CEMS findings of the ε-nitride phase [ε-$(Fe,Cr,Mn)_{2+x}N$] correlate quite well with those of the XRD results [Figs. 3.6 and 3.7]. The close examination of the Mössbauer results for the high dose N implanted specimen reveals an important finding related to the orientation of ε-nitride grains in the implanted layer. The unequal line intensities for the paramagnetic component (Δ = 0.37, see Fig. 3.9 and Table 3.3) are due to non-random distribution of electric field gradients caused by a preferred orientation of the hexagonal phase [51,52]. In fact, our XRD results, particularly for the high dose N implanted sample (Fig.3.7) suggests a preferential (100 and 002) orientation of ε-nitride grains (located at 39° and 42° in 2θ) parallel to the surface based on the comparison of the relative intensities at increasing incident angles and the absence of other reflections.

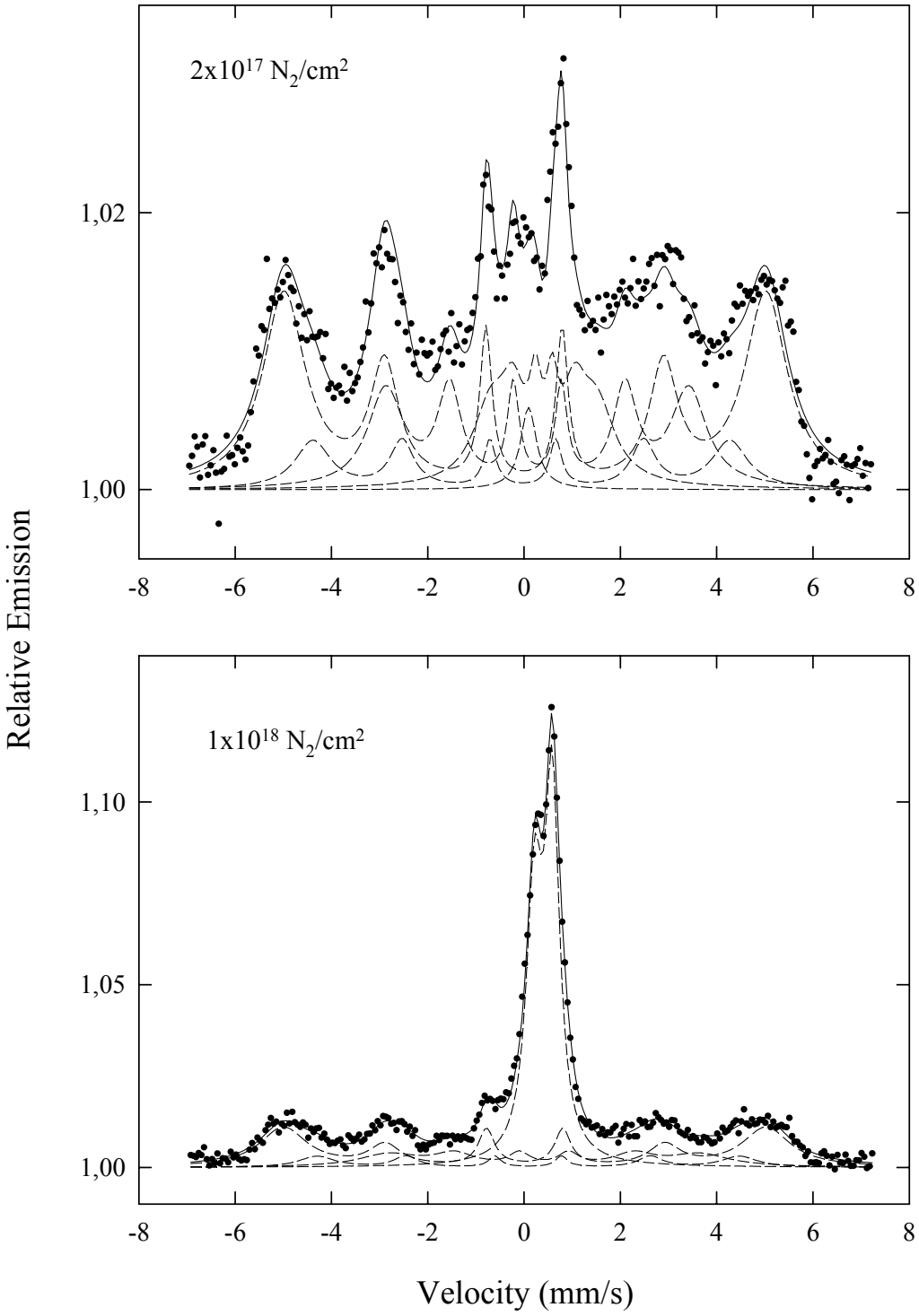

Figure 3.8. CEMS data and the computer fits for the nitrogen ion implanted specimens SC7 and SC18 at $2x10^{17}$, $1x10^{18}$ ions/cm^2, respectively. The data for the SC7 were rather complex, while a strong paramagnetic component is dominant in SC18.

CHAPTER 4

CROSS-SECTIONAL SEM AND OPTICAL MICROSCOPY ANALYSES

4.1 Cross-Sectional SEM Analysis

4.1.1 Plasma Nitrided Specimens

Cross-sectional SEM analysis was done on selected plasma ion nitrided and nitrogen ion implanted specimens. Figures 4.1, 4.2, and 4.3 show the SEM results for the plasma ion nitrided specimens SC10, SC3, and SC14 corresponding to the N_2/H_2 gas flow ratios of 1/10, 1/1, and 3/1, respectively.

The cross-sectional SEM results corresponding to the N_2/H_2 = 1/10 gas mixture specimen are shown in Fig. 4.1. The top photomicrograph in this figure indicates two distinct regions, one of which the nitrided layer (diffusion layer) phase attacked strongly by the chemical etch used (nital) and the other, the substrate phase, is mainly attacked along the grain boundaries. The upper photomicrograph in Fig. 4.1 clearly reveals the nitrided layer with a relatively uniform layer thickness. Regarding the nitrided zone morphology, this figure shows that a well-defined planar interface between the nitrided zone and the substrate was developed. The lower photomicrograph with a higher magnification of the same region as in the upper picture taken along the nitrided layer clearly reveals the microstructure of the nitrided layer under the N_2/H_2 = 1/10 conditions. This picture when examined carefully shows that the nitrided layer (diffusion zone) is composed of fine precipitates of CrN. This photomicrograph was taken after using Vilella's reagent (15 ml glycerol, 15 ml nitric acid and 30 ml hydrochloric acid). The nitrided layer thickness is estimated from the pictures in Fig. 4.1. The photomicrographs in Fig. 4.1 represent two of several pictures taken along the nitrided layer. Careful analysis of the several pictures reveal the nitrided layer microstructures with thicknesses as low as 17 μm and as high as 20 μm. Note that, the

thin bright band on the top is due to charging at the boundary between the sectioned surface and the bakelite.

Figure 4.2 shows the SEM results for the specimen plasma ion nitrided under the N_2/H_2=1/1 gas flow ratio. The upper photomicrograph is composed of two distinct regions, one of which (the compound layer) has a thickness ranging from 7 to 12 μm with a good etch resistance, and the other (the diffusion layer) with a thickness range from 120 to 130 μm and with a relatively poor etch resistance. The compound layer consists of the ε-nitride, γ'-nitride, the cementite-like phase, and CrN based on the XRD, CEMS and CXMS results for this sample while the diffusion layer is mainly composed of fine precipitates of CrN based on the SEM results. The lower photomicrograph in Fig. 4.2 with a higher magnification of the same region as in the upper picture taken along the nitrided layer clearly reveals the morphology of the compound and diffusion layers. The SEM picture indicates a nonuniform dendritic type of growth behaviour for the compound layer while the diffusion layer shows a uniform profile extending deeper into the material. The average total nitrided layer (compound layer + diffusion layer) thickness for the N_2/H_2=1/1 conditions thickness is found to be about ~135 μm.

One key observation related to the lower hand side of the upper photomicrograph in Fig. 4.2 is that this region is strongly attacked by the etchant used (nital). This flake-like shaped area contains sulphur and manganese rich regions based on the EDX analysis. It is believed that the relatively poor corrosion resistance of the bulk material (the substrate phase) is attributed to these regions since they serve as corrosion initiation centers and reduce the overall corrosion resistance of the high chromium steel used in this study. This property of the material is further supported by the steel company, Assab Korkmaz, which provided us the material for this research.

The SEM analysis results for the plasma nitrided specimen (SC14) under the N_2/H_2 = 3/1 gas flow rate conditions are shown in Fig. 4.3. The upper micrograph (taken after etching by nital) in this figure clearly shows the uniform nature of the nitrided layer while the lower photomicrograph (taken after etching by Vilella's reagent) with a higher magnification of the same region as in the upper picture taken along the nitrided layer clearly reveals the morphology of the nitrided layer. The XRD, CEMS and CXMS results indicate the existence of the compound layer forming phases distributed along the top nitrided layer. However, based on the SEM results the nitrided layer consists

mainly of the diffusion layer only. Although the bottom picture in Fig. 4.3 reveals the existence

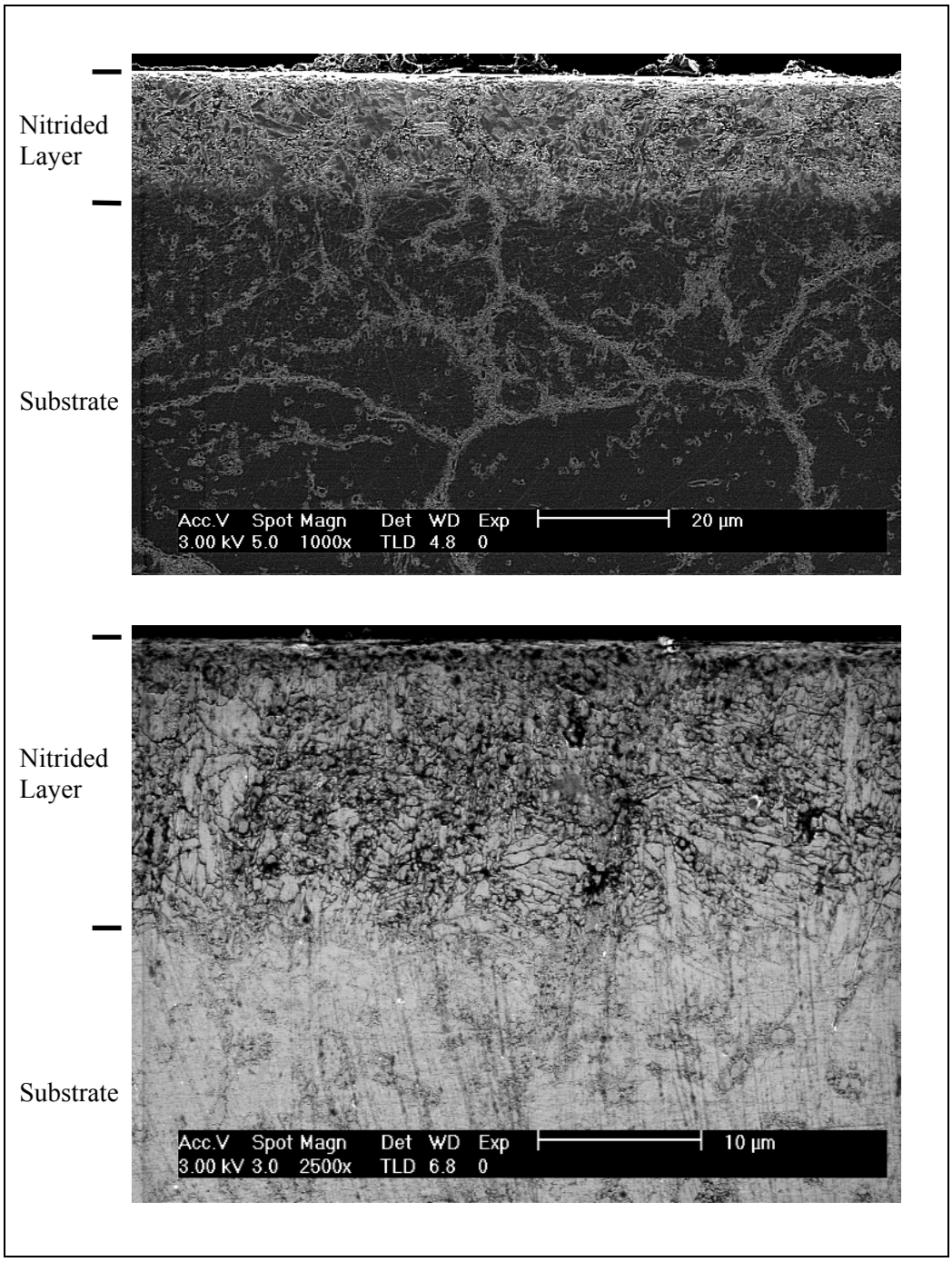

Figure 4.1. Cross-sectional SEM data for the plasma ion-nitrided specimen with the gas composition N_2/H_2 = 1/10. The photomicrographs refer to the same region of the nitrided layer. Note that the lower photomicrograph clearly reveals the microstructure with coherent nitride precipitation (CrN) formation in the nitrided zone.

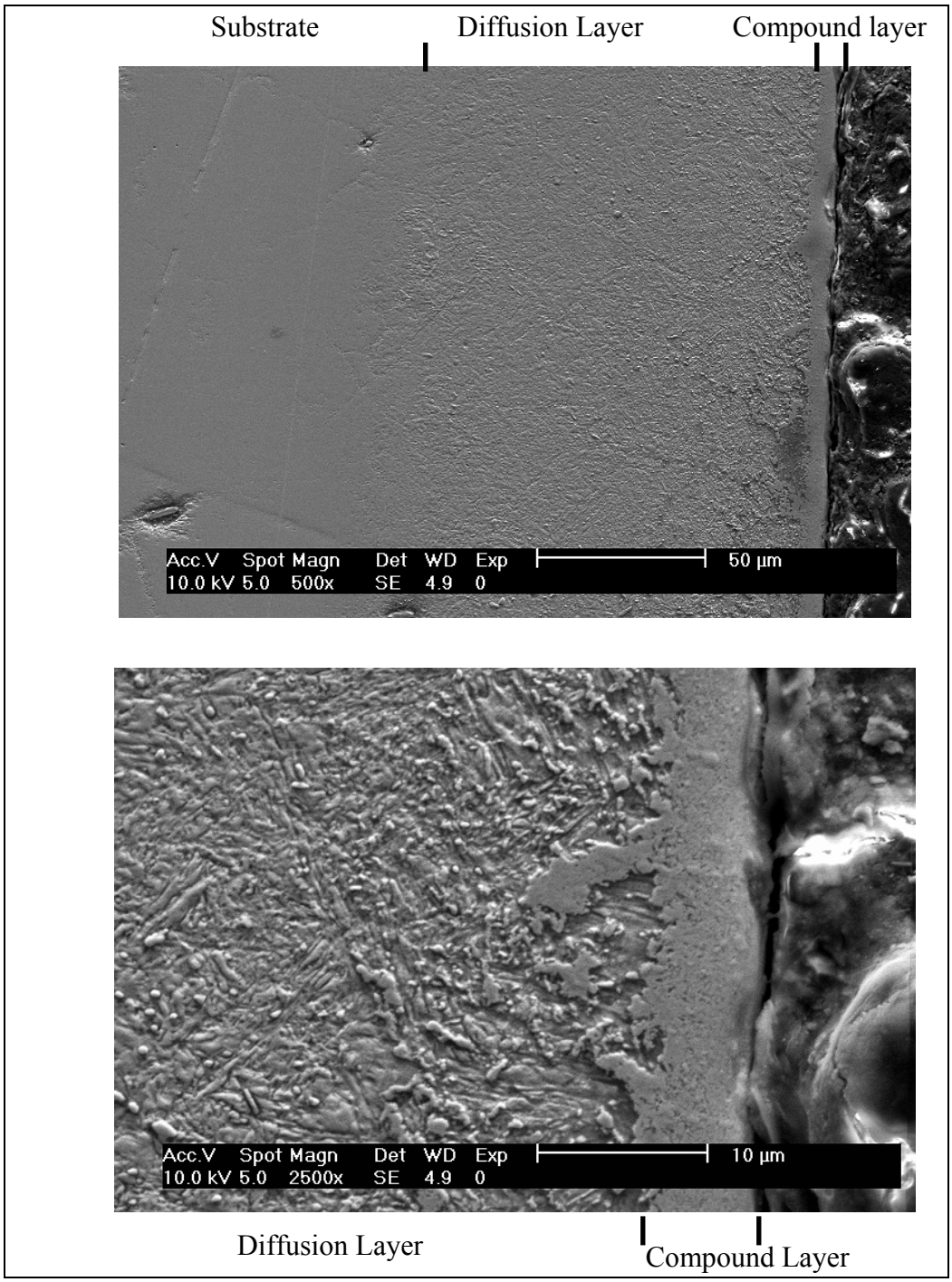

Figure 4.2. Cross-sectional SEM data for the plasma ion-nitrided specimen with the gas composition N_2/H_2 = 1/1. The lower photomicrograph with a higher magnification of the same region as in the upper picture taken along the nitrided layer clearly reveals the morphology of the compound and diffusion layers.

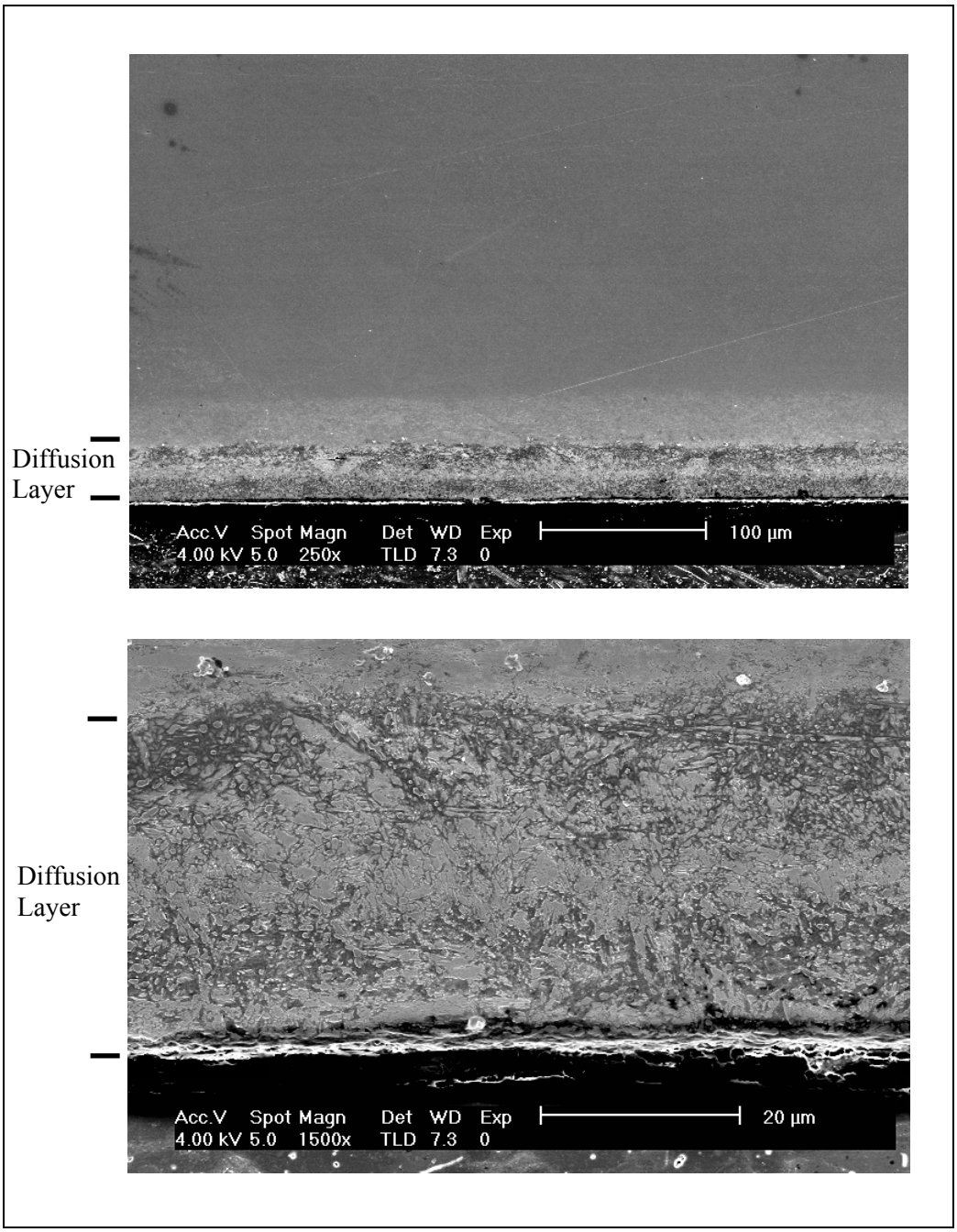

Figure 4.3. Cross-sectional SEM data for the plasma ion-nitrided specimen with the gas composition N_2/H_2 = 3/1. The lower photomicrograph with a higher magnification of the same region as in the upper picture taken along the nitrided layer clearly reveals the morphology of the nitrided layer

of some etch resistant regions located close to the surface, no compound layer formation is found for the specimen (SC14) plasma nitrided under the N_2/H_2 = 3/1 conditions compared to the specimen nitrided under N_2/H_2 = 1/1 conditions. This might be attributed to the intense sputtering taking place during the nitriding of this sample. The RMS roughness value for this sample is ~ 0.84 μm in comparison to the as-polished sample with ~ 0.02 μm. The lack of formation of the compound layer for the N_2/H_2 = 3/1 conditions might also be due to reduced amount of H_2 in the plasma [14,15].

A careful inspection of the photomicrographs reveal that the diffusion layer thickness of the plasma nitrided specimen under N_2/H_2 = 3/1 gas flow ratio based on the several regions, obtained from the several photomicrographs is about 40 μm. Note here that the thin bright band on the bottom picture in Fig. 4.3 is due to charging at the boundary between the sectioned surface and the bakelite.

In conclusion, the thickest nitrided layer is found to be about 135 μm and is obtained for the nitriding under N_2/H_2 = 1/1 gas flow ratio conditions while the thinnest is about 20 μm and is found for the nitriding under N_2/H_2 = 1/10 gas flow ratio conditions. Increasing the gas flow ratio higher N_2/H_2 = 3/1 did not result in thicker layers. It can be concluded that the depth of the nitriding zone increases by increasing the nitrogen gas flow ratio up to some critical value and beyond this value, it starts to decrease. This behaviour could be explained by the fact that the growth of the nitrided layer is not only determined by the inward movement of the nitrogen from the surface, but also adversely affected by the sputtering effect [10] as indicated previously for the specimen nitrided under N_2/H_2 = 3/1 gas flow ratio.

It is found that the N_2/H_2 = 1/1 conditions produces the thickest nitrided layer. Part of this thickness may be due to the larger nitriding time and temperature for this set of conditions. As can be seen from Table 2.2, this set of samples (SC3, SC4, SC5, SC6) were nitrided 3 hours longer than other sets of samples add the nitriding temperature for the same set of samples was also 20 °C higher compared to the other sets.

To reveal the possible effects of the differences in the nitriding conditions, we assume a diffusion-controlled N penetration depth $X \sim (Dt)^{1/2}$, where t is the process time at temperature T, and D is the diffusion coefficient at T. The diffusion coefficient D of N in pure bcc α-Fe can be represented by $D(T) = D_o Exp[-E/k_bT]$, where D_o (=0.03 cm^2s^{-1}) is the prefactor, and E (=0.79 eV/atom) is the activation energy of the N [53]. The difference in the diffusion coefficients due to the difference in nitriding conditions

are obtained as D(520 °C) = 2.9x10^{-8} cm^2/s, and D(540 °C) = 3.8x10^{-8} cm^2/s. Under the N_2/H_2 = 1/1 nitriding conditions (see Table 2.2), the N penetration depth is estimated and found to be X(t=18 h; T=540 °C) ≅ 1.25 X(t=15 h; T=520 °C). This analysis predicts that the nitrided layer depth under the N_2/H_2 = 1/1 conditions should approximately be 25 larger due to the larger nitriding time (18 h) and higher nitriding temperature (T=540 °C) compared to the other nitriding conditions.

However, the predicted N depth based on X ~ $(Dt)^{1/2}$, should be much smaller since the N is not diffusing through bcc pure Fe but through bcc an FeCr material with significant amount of Cr (16.7 wt. % Cr). It is known that nitrogen penetration is significantly affected by the existence of the nitride forming elements. Cr, for example, has strong affinity for nitrogen and drastically reduces the diffusion of nitrogen [53]. The literature studies [6,9,18,43] find that the growth kinetics of plasma nitrided layers is similar to that observed for gas nitrided alloys, i.e. the thickness of nitrided layers increased with the square root of time and the inverse of the chromium contents.

4.1.2 N Ion Implanted Specimens

The cross-sectional SEM data for the low (2x10^{17} ions/cm^2) dose and high (1x10^{18} ions/cm^2) dose N implanted specimens (corresponding to SC7 and SC16, Table 2.3) are given in Fig. 4.4. Both photomicrographs reveal the N implanted layer with a relatively uniform thickness. The upper photomicrograph (2x10^{17} ions/cm^2 sample) gives the nitrogen ion implanted thickness to be in the range of 0.03 to 0.05 μm. The N ion implanted layer thickness based on the SEM photomicrograph (the lower picture) related to the specimen SC16 and implanted to the dose of 1x10^{18} ions/cm^2 is in the range of 0.05 to 0.08 μm. The implantation depths obtained by the SEM analysis are consistent with the range of implanted N ions (which is ~ 90 nm for 85 kV ion energies) predicted by the TRIM (Transport of Ions in Materials) Model [50]. These results also agree quite well with the N implanted layer thicknesses obtained from the Mössbauer results, which were 65 nm for the high dose and 40 nm for the low dose implantation.

The etching time was critical for obtaining SEM photomicrographs of the specimens for the simple reason that not only the N implanted layer is extremely thin but also the chemical etch used (HCl+ H_2O_2) was quite strong.

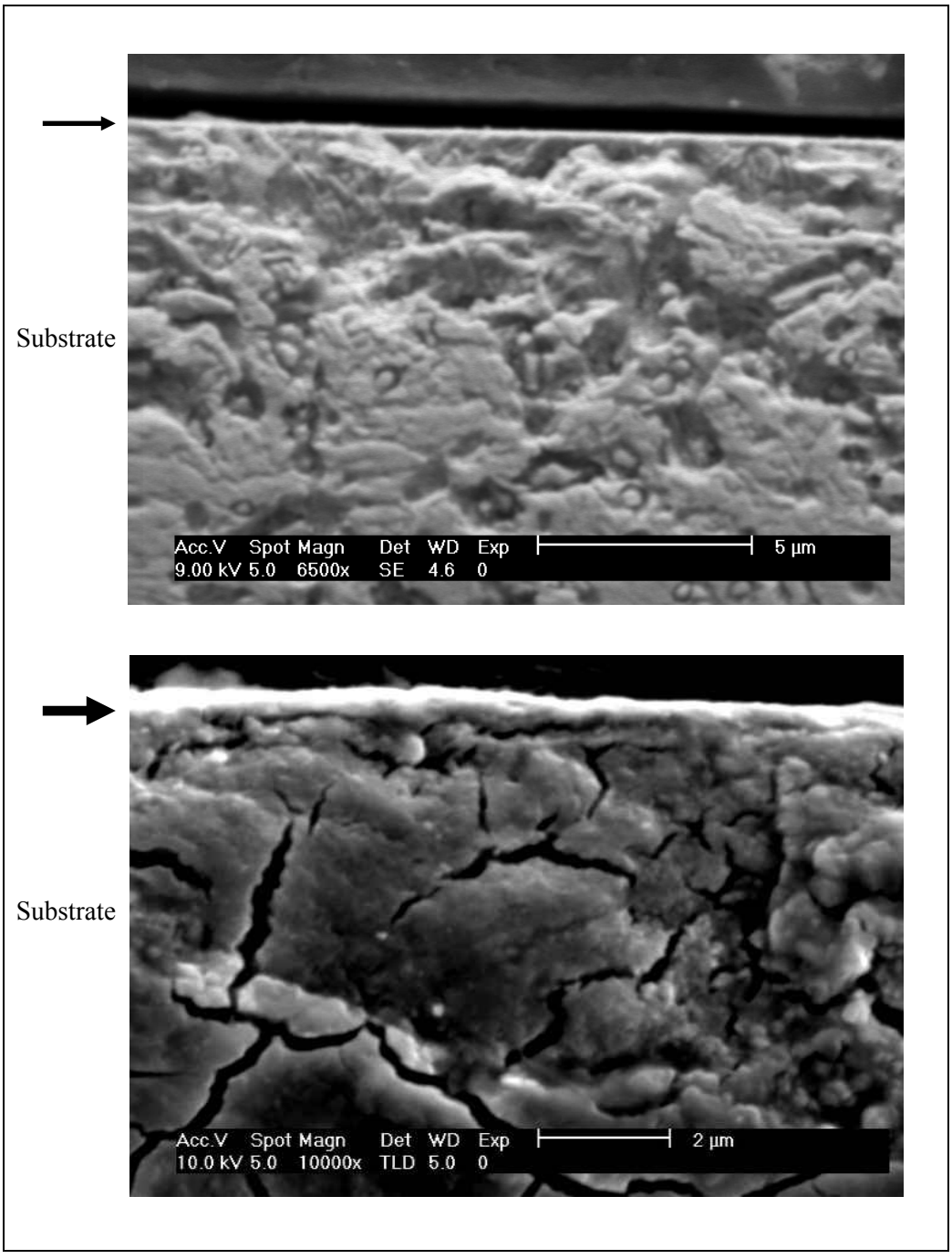

Figure 4.4. Cross-sectional SEM data for the nitrogen ion implanted specimens at doses of (a) $2x10^{17}$ and (b) $1x10^{18}$ ions/cm^2, respectively. Arrows in the pictures indicate the nitrogen ion implanted layers. Note that the chemical etch used strongly attacks the substrate, α-(Fe, Cr, Mn), while the N implanted layer is almost unaffected.

Note that the chemical etch used (HCl + H_2O_2) strongly attacks the substrate phase [α-(Fe,Cr,Mn)] while the implanted layer phase determined by XRD and Mössbauer analysis, ε-$(Fe,Cr,Mn)_{2+x}N$, is almost unaffected by the same etch indicating strong etch resistance of the N implanted layer phase.

The SEM analysis of the N implanted specimens was rather difficult due to the strong magnetic behaviour of the substrate material compared to the SEM analysis of the nitrided specimens, especially when the SEM was used in the ultrahigh resolution (UHR) mode. The interaction between the specimens and the magnetic field in the SEM unit was so strong that the bakelited metal sample was coming out of the sample stage. Even after fixing the specimen to the sample stage it is still impossible to analyse the specimen under the UHR mode. It was observed that even at near the limit of the high resolution (HR) mode, the quality of the photomicrographs were significantly poor. So, the analysis of the implanted specimens by SEM was limited.

4.2 Optical Microscopy Analysis

Optical microscope (OP) analysis in the DIC illumination mode was also used in combination with SEM analysis. Figure 4.5 shows optical microscope images of the specimen SC3 plasma ion nitrided under N_2/H_2=1/1 gas flow ratio. The photomicrographs in Fig. 4.5 were taken after fine polishing step (before etching). They indicate two distinct regions, one of which is the nitrided layer and the other, the substrate phase. The photomicrographs clearly reveal the nitrided layer with a relatively uniform layer thickness. The thickness of the nitrided layer obtained from several photomicrographs is found to be about ~125 μm and agrees quite well with that obtained by the SEM results for this sample. Note that the topographic details in these pictures are revealed vividly under the DIC illumination mode while the boundary between the nitrided layer and the substrate is almost invisible under bright field illumination.

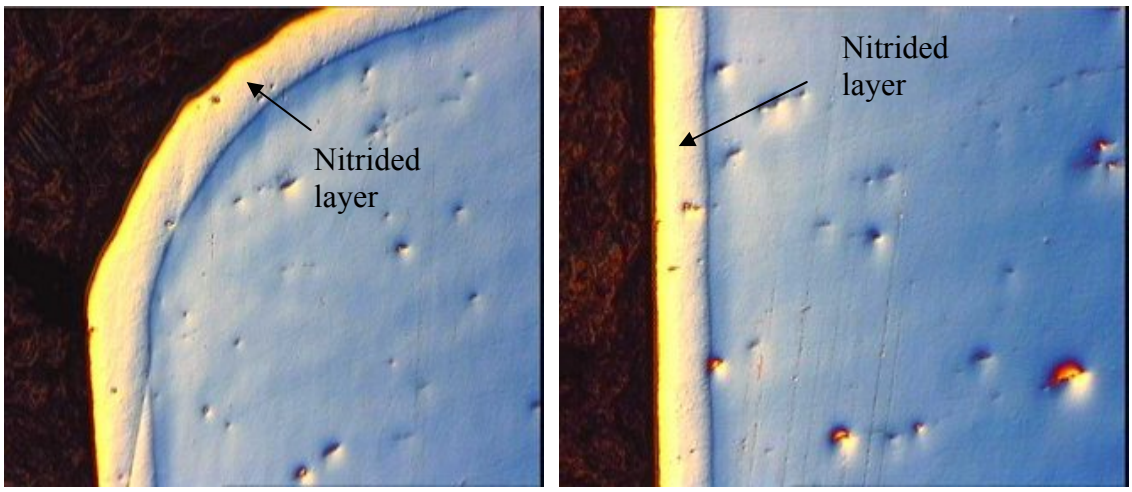

Figure 4.5 Optical microscope images showing the surface morphologies of the nitrided specimen under N_2/H_2 = 1/1 gas flow ratio. These photomicrographs were taken by using DIC illumination mode after fine polishing step (no etching).

CHAPTER 5

MICROSTRUCTURE CORRELATION WITH MECHANICAL PROPERTIES

5.1 Surface Roughness Measurements

The surface roughness measurement results for the plasma ion nitrided and the nitrogen ion implanted specimens as well as the as-polished sample are listed in Table 5.1. Also summarized in this table are the nitrided and N implanted layer thicknesses based on the SEM photomicrographs. The roughness values given in this table are the average values for each specimen. Note that the significant changes in root mean square (RMS) roughness values are observed for the plasma ion nitrided specimens on contrary to the nitrogen ion implanted specimens. Note also that the higher gas flow ratio results in higher surface roughness for the nitrided specimens, in particular for the samples nitrided under N_2/H_2 = 3/1 gas flow conditions. The increase in the surface roughness can be explained by the fact that at high nitrogen gas flow ratios the sputtering rate of the nitriding process increases resulting in a poorer surface finish quality for the samples. As can be inferred from Table 5.1, the sputtering rate increases with increasing relative abundance of nitrogen in the plasma.

The RMS roughness values for the N implanted specimens are quite small (close to the RMS roughness values for the as-polished specimen), and this suggests that no significant sputtering occurs during the nitrogen ion implantation. In general terms, conventional ion implantation is considered to be a gentle and very safe surface treatment for it has no influence on surface finish, tool shape and dimensions due to low process temperatures.

Table 5.1. The root mean square roughness values (RMS) for the plasma ion nitrided and nitrogen ion implanted specimens. Note that the related surface treatment and the treatment-induced thicknesses are also indicated in detail to visualise the relation.

Treatment and the Specimen #	Treatment Detail	RMS (μm)	Case Depth (μm)
As-Polished	-	0.02 ± 0.01	
Plasma Nitriding	Gas flow ratio (N_2/H_2)		
SC10, SC11, SC12	1/10	0.12 ± 0.01	17-20
SC3, SC4, SC5, SC6	1/1	0.40 ± 0.05	120-130
SC13, SC14, SC15	3/1	0.84 ± 0.10	38-42
N Ion Implantation	Dose (ions/cm^2):		
SC7, SC8, SC9	$2x10^{17}$	0.04 ± 0.00	≈ 0.05
SC10, SC11, SC12	$1x10^{18}$	0.05 ± 0.00	≈ 0.08

5.2 Nanohardness Measurements

The hardness of the substrate was measured by a microhardness tester under an applied load of 100 g (HV1), and found to be 350 HV. This hardness value for the base material is used as a reference value for the hardness values for the nitrided and nitrogen ion implanted layers. One has to note that the following results to be discussed are based on the relative increases in hardness values (of the nitrided and the nitrogen ion implanted layers in comparison to the substrate material) since the measured hardness values are only relevant in terms of the relative hardness values due to the strain rate sensitivity of the bulk material.

The cross-sectional nanohardness depth profiling measurements of the plasma ion nitrided specimens are shown in Fig. 5.1 for the applied load of 10 mN [1g, (HV 0.01)]. The results clearly indicate that the surface hardness (which is defined as the hardness value obtained from the position nearest to the plasma nitrided surface) of the nitrided specimens is increased by about a factor of 3 in comparison to that of the bulk material and the hardness depth profile is found to be plateau-shaped, in particular for the plasma nitrided specimens under the N_2/H_2 = 1/1 and 3/1 gas flow conditions.

This distinct characteristic is normally associated with the hardness profiles of high chromium steels and is attributed to the strong interaction nature of the Cr. From

the hardness-depth profiles, the hardness depth (defined as the depth at which the hardness has decreased to half its near surface value) is estimated to be 25, 50, and 150 μm for the N_2/H_2=1/10, 3/1, and 1/1 nitrided specimens, respectively. These depths correlate quite well with the nitrided layer thicknesses obtained by the cross-sectional SEM analysis results. The smaller case depth for the N_2/H_2=3/1 specimen is explained by the fact that at higher gas flow ratios (higher nitrogen fluxes), sputtering rate becomes significant. The nitrided layer growth is mainly a diffusion controlled process. However, at high nitrogen fluxes the sputtering rate impedes the growth of the nitrided layer [25].

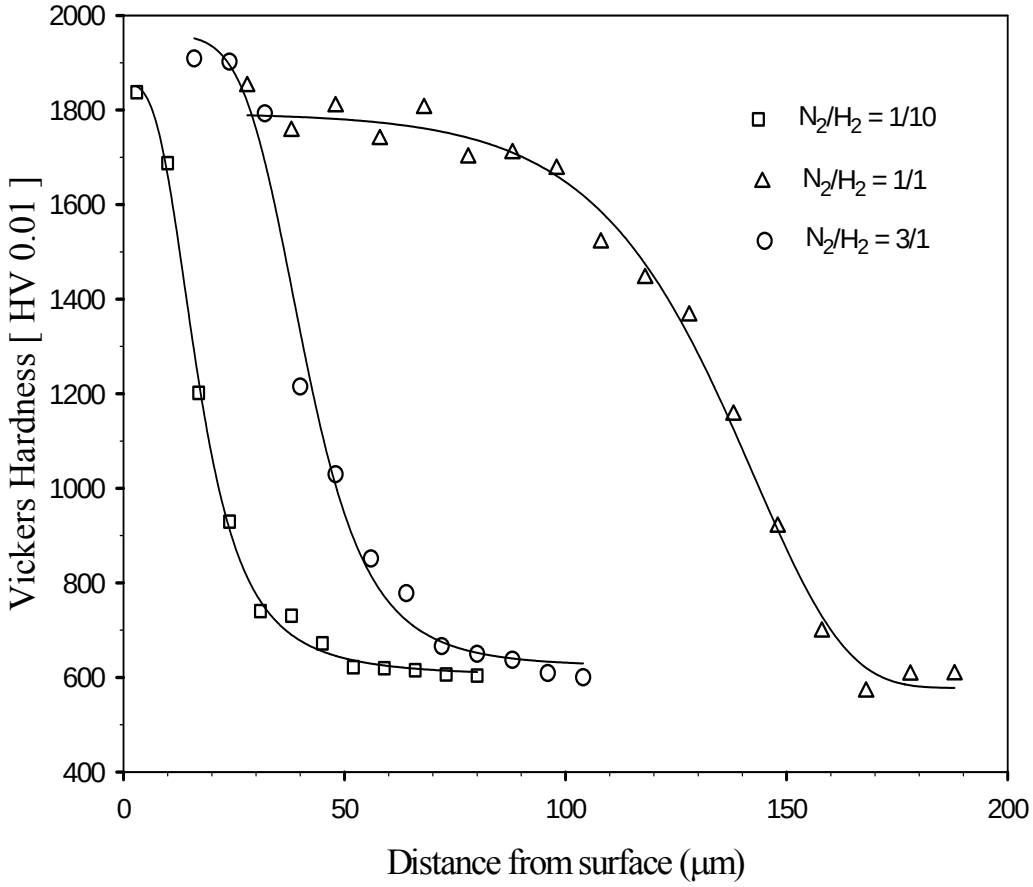

Figure 5.1. The cross-sectional nanohardness measurements results of the plasma ion nitrided specimens. Note that the formation of maximum hardness plateau is very important characteristics of the hardness profiles of the high chromium steel.

In conclusion, plasma nitriding and N ion implantation produces surface layers with improved hardness. There may a number of mechanisms contributing to the

enhanced hardness behaviour of the nitrided and the N implanted layers such as: the solid solution hardening, dislocation hardening and/or the precipitation hardening. In ferrite, combination of nitrogen with chromium and iron leads to precipitation of nitrides. As a result, the hardening effect is, therefore, due to a fine homogenous coherent nitride precipitation (CrN, ε-Fe_3N and γ'-Fe_4N) which is confirmed by XRD and cross-sectional SEM analysis. The formation of maximum hardness plateau is very important characteristics of the hardness profiles of high chromium steels [19]. The hardness is only slightly changed by the nitrogen in solid solution, while the hardness increases substantially when the nitride precipitations form, depending on the nitride-forming alloying elements [6]. As a consequence, this plateau is believed to be associated with the nitrogen compositional profile through the nitrided surface.

The surface nanohardness values as a function of indenter load for the nitrogen implanted specimens are given in Fig. 5.2. The hardness values at the lightest load (0.5g) show that the surface hardness values of the high dose implanted specimen and the low dose implanted specimen are increased by more than a factor of 1.6 and 1.4, respectively, in comparison to the bulk material. One important feature here is that the average penetration depths of the tip of the indenter at the lightest load (0.5 g) are 0.15 and 0.16 μm for the high and the low dose implantation, respectively, and these values exceed the implanted layer thicknesses (the average implantation depths obtained by the Mössbauer analyses for these specimens are about 40 and 65 nm). Therefore, these surface hardness values are not truly representative of the N implanted layer and the true hardness values of these layers should be much higher than what is found.

These hardness results are in good correlation with the SEM, XRD and CEMS analyses, in that, the SEM results for the higher dose sample show thicker nitrogen implanted layer and both CEMS and XRD/GIXRD results also verify that the higher dose sample has thicker, ε-$(Fe,Cr,Mn)_{2+x}N$ phase with more nitrogen.

The hardness values in Fig. 5.2 continuously decrease to smaller values at larger indenter loads approaching the hardness value of the substrate phase. This can be explained by the fact that at higher indentation loads the penetration depth of the indenter increases resulting in more and more contribution from the substrate phase.

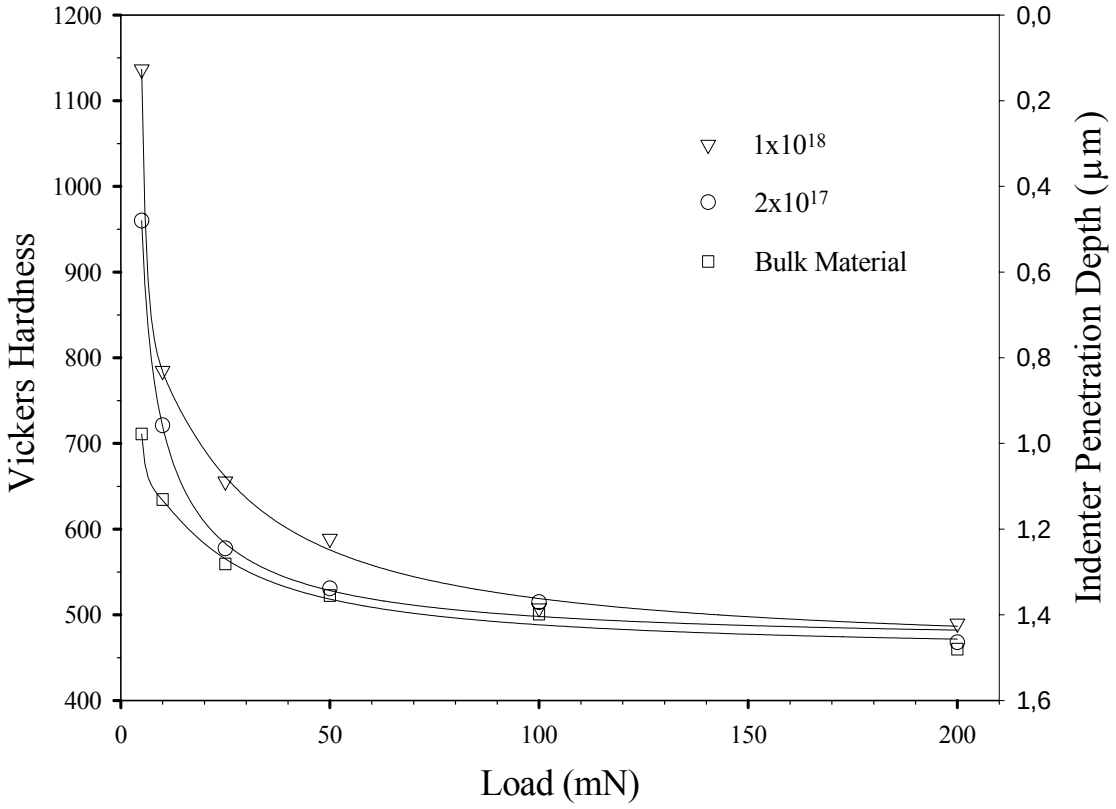

Figure 5.2. Surface nanohardness measurement results of the as-polished and the N implanted specimens. The penetration depth values shown on the right hand side are only given for the high dose ($1x10^{18}$ ions/cm^2) N implanted specimen.

In addition to the surface hardness values, the cross-sectional hardness-depth profiles for the N implanted specimens were also obtained and the results are shown in Fig. 5.3. In order to obtain meaningful data, the measurements were carried out using the lightest load available (0.5g) in this system. As can be seen from this figure, the hardness values near the surface for the high dose N implanted specimen has increased by a factor of 2.2 in comparison to the substrate value. The increased hardness value correlates quite well with the previous results (XRD/SEM/CEMS) indicating a uniform layer of ε-nitride [ε- $(Fe,Cr,Mn)_{2+x}N$] distributed in the N implanted layer.

In the case of N ion implanted specimens, the enhanced hardness is attributed to the formation of ε-$(Fe,Cr,Mn)_{2+x}N$ phase, and to compressive residual stresses, caused by the distortion of the lattice due to N in interstitial sites, and also due to the volume expansion in the case of precipitates through the implanted layers. The latter arises from the observation of the XRD/GIXRD peaks of the nitrogen implanted specimens. The strongly broadened peaks of the ε-phase in the N implanted specimens show an asymmetry toward higher diffraction angles, suggesting a nonuniform nitrogen

distribution or concentration gradient in the implanted layer. There will be, therefore, a residual stress profile, closely associated with the N concentration profile as a function of depth [52]. The cross-sectional hardness measurement result in Fig. 5.3 indicates the results of such residual stress formation since the increased surface layer hardness values come from beyond the range of the implanted layer. It is well known in the literature [54] that the influence of the accelerated ion beams is not limited to implanted zone only. The modification of the structural-phased state (the formation of dislocation structures and stresses) can take place in the subsurface layers located well beyond the implanted zone. The subsurface layer with the modified structural-phased state is called the ion-affected zone. According to the literature [54], the thickness of the ion effected zone increases with increasing dose. Our result show that the high dose implanted specimen has deeper hardness distribution (see Fig. 5.3) is consistent with this finding.

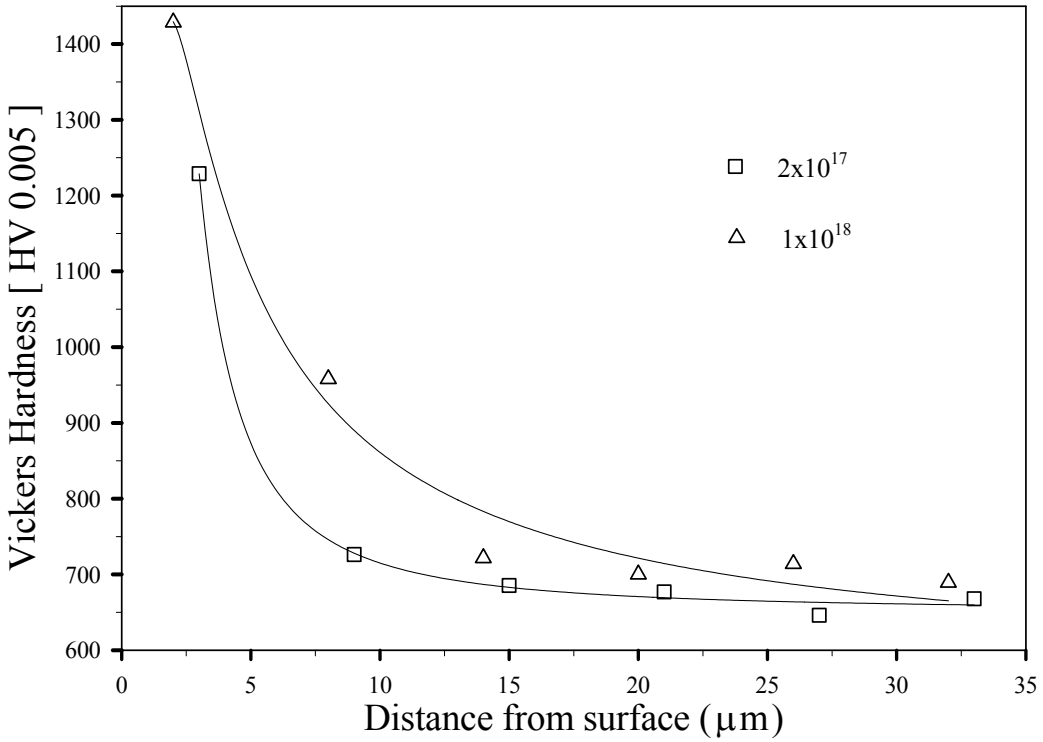

Figure 5.3. Cross-sectional nanohardness measurement results of the N implanted specimens. Note that the results are in correlation with the surface nanohardness measurements.

5.3 Wear and Friction Measurements

Figures 5.4, 5.5 and 5.6 show the friction and wear analyses results for the as-polished (the substrate), the nitrogen implanted and the plasma ion nitrided specimens. The quantitative results associated with these analyses are also given in Table 5.2.

The coefficient of the friction values (Table 5.2) are found to decrease for the N implanted specimens in comparison to the friction coefficient value for the as-polished sample. This decrease is about 12 % for both the low dose and the high dose N implanted specimens. The friction analysis results shown in Fig. 5.4 have some common features in that the coefficient of friction initially rises steeply, and then shows a tendency to stabilize. The friction behaviour for the low dose N implanted sample ($2x10^{17}$ ions/cm^2) shows a drastic change over 3200 laps implying that the N implanted layer has failed. On the other hand, the high dose ($1x10^{18}$ ions/cm^2) nitrogen implanted specimen shows quite a stable friction behaviour for the duration of the experiment (5000 laps).

As can be seen from Table 5.2 and Fig. 5.5, the coefficient of friction values are much smaller for the plasma nitrided specimens compared to those of the as-polished and as-implanted samples. For example, the friction coefficient value for the N_2/H_2 = 1/1 is 0.77 and this represents 22 % drop with respect to the substrate material. Figure 5.5 shows that the friction behaviour for the nitrided specimens are also quite stable over the period of the experiments (5000 rotations).

One interesting key feature of the friction profiles is that the starting friction (μ_s) values for the nitrogen implanted specimens are much lower than those of the plasma nitrided specimens (Table 5.2 and Figs. 5.4 and 5.5). This can be explained by the fact that initially the nitrided samples had a much larger RMS roughness than the N implanted specimens. This result points out that the μ_s values are mainly determined by the surface roughness.

Another key observation related to the friction profiles of the plasma nitrided specimens in Fig. 5.5 is that these profiles show a very small tendency to decrease in μ values after reaching the highest value. And this slow but gradual decrease in the friction coefficient during the experiment is typical in wear process, in which the surface roughness decreases and the effective contact area between stationary ball and rotating sample increases [21].

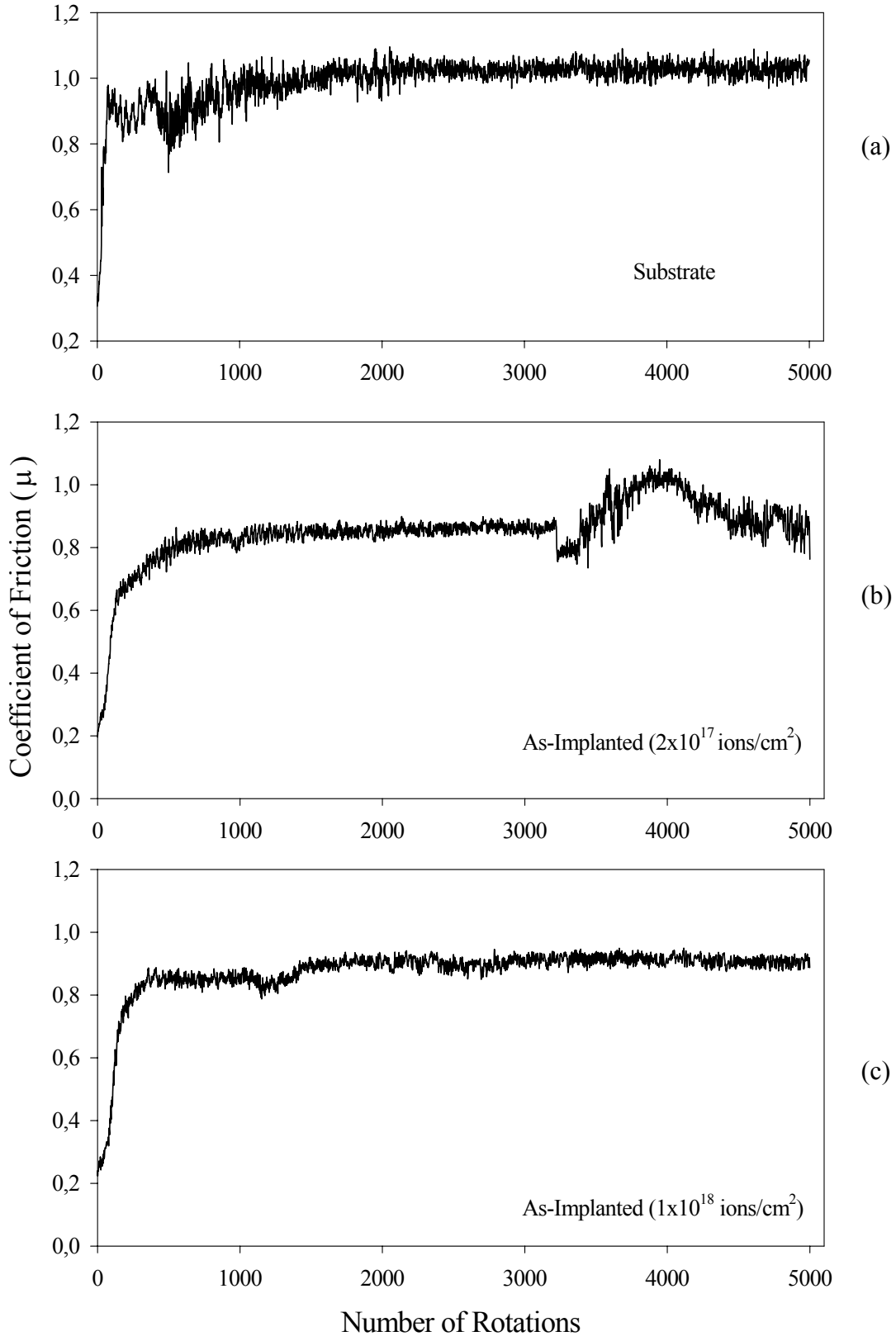

Figure 5.4. Friction behaviour of the (a) as-polished and the nitrogen ion implanted specimens at doses (b) $2x10^{17}$ and (c) $1x10^{18}$ ions/cm^2 under dry cyclic sliding motion with humidity controlled through nitrogen atmosphere.

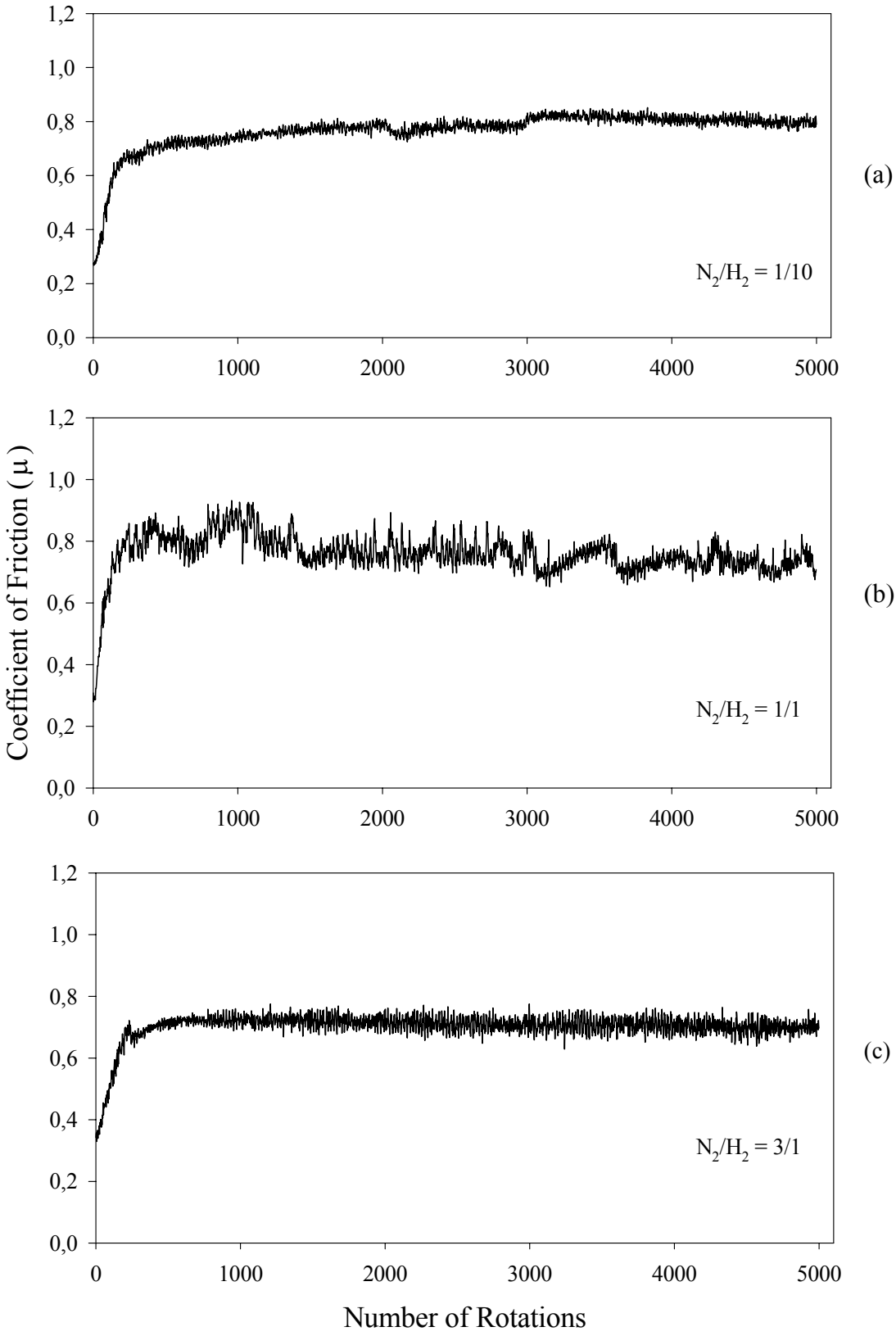

Figure 5.5. Friction behaviour of the plasma ion-nitrided specimens under (a) N_2/H_2=1/10, (b) 1/1, and (c) 3/1 gas flow ratios under dry cyclic sliding motion with humidity controlled through nitrogen atmosphere.

Table 5.2. The experimental results associated with the friction and wear analyses.

	Starting friction (μ_s)	Friction coefficient (μ_{avg})	Wear trace area (μm^2)
As-polished	0.38	0.99 ± 0.08	1,3
Ion nitriding (N_2/H_2)			
1/10	0.43	0.75 ± 0.08	Not observed
1/1	0.44	0.77 ± 0.08	Not observed
3/1	0.48	0.80 ± 0.05	Not observed
N implantation (ions/cm^2)			
$2x10^{17}$	0.30	0.87 ± 0.11	0.2
$1x10^{18}$	0.33	0.85 ± 0.09	Not observed

When we compare the coefficient of friction values of the N ion implanted specimens at different doses, we observe no significant change. This result clearly demonstrates that increasing the ion dose does not induce further increase in the coefficient of friction, whereas, we believe that the dose mainly increases the load bearing capacity of the layer itself.

According to the results, it was found that the plasma nitrided layers decreases the coefficient of friction more than the nitrogen ion implanted layers. This result seems a bit confusing since the plasma ion nitriding induces significant changes on the roughness of the surface due to sputtering. The observed decrease in the coefficient of friction, however, could be attributed to the nitride formation, which is well documented in the literature, [29].

Figure 5.6 shows the wear trace morphologies (obtained by surface profilometry) for the as-polished, the N ion implanted, and the plasma nitride specimens and the quantitative results associated with the wear track area analysis are given in Table 5.2. The average wear trace area (Table 5.2) is found to be significantly reduced for the N ion implanted specimen ($2x10^{17}$ ions/cm^2) in comparison to the wear trace area of the as-polished sample. As can be seen from Table 5.2, the wear trace area of the low dose N implanted sample is 0.2 μm^2, and this represents an 85 % drop with respect to the substrate (the wear trace area of the substrate is 1.3 μm^2).

The wear trace analysis as well as the wear trace morphology of the high dose implanted specimen ($1x10^{18}$ ions/cm^2) shown in Fig. 5.6c and Table 5.2 indicates that almost no wear is observed over the period of the ball-on disk wear analysis experiments (5000 rotations) under a contact pressure of about 100 MPa.

Similar to the high dose implanted specimen, the plasma nitrided specimens also represent excellent wear resistance over the period of the wear analysis almost no wear is observed for all the nitrided specimens. Figure 5.6d shows an interesting feature associated with the wear trace morphology of the plasma nitrided specimens. The region indicated by an arrow in Fig. 5.6d is the region of the wear trace (where the wear is taking place). As can be seen from this region, there is a decrease in surface roughness. The decrease in surface roughness increases the effective contact area between stationary ball and rotating sample. This finding is in good agreement with the observed, gradual but slow decrease in the friction coefficients of the plasma nitrided samples as explained previously.

In conclusion, the wear resistance of the bulk material is enhanced through N ion implantation and plasma ion nitriding. Furthermore, the higher dose implantation is found to be more effective in increasing the wear resistance. Reduction in wear obtained with N implantation and plasma nitriding is generally thought to result from the strengthening of the metal near the wearing surface [27]. The observed relative increase in the wear resistance of the ion implanted samples are in good agreement with the observed hardness profiles in that the high dose N implanted specimen has higher surface hardness as well as a hardness-depth profile extending deeper into the substrate.

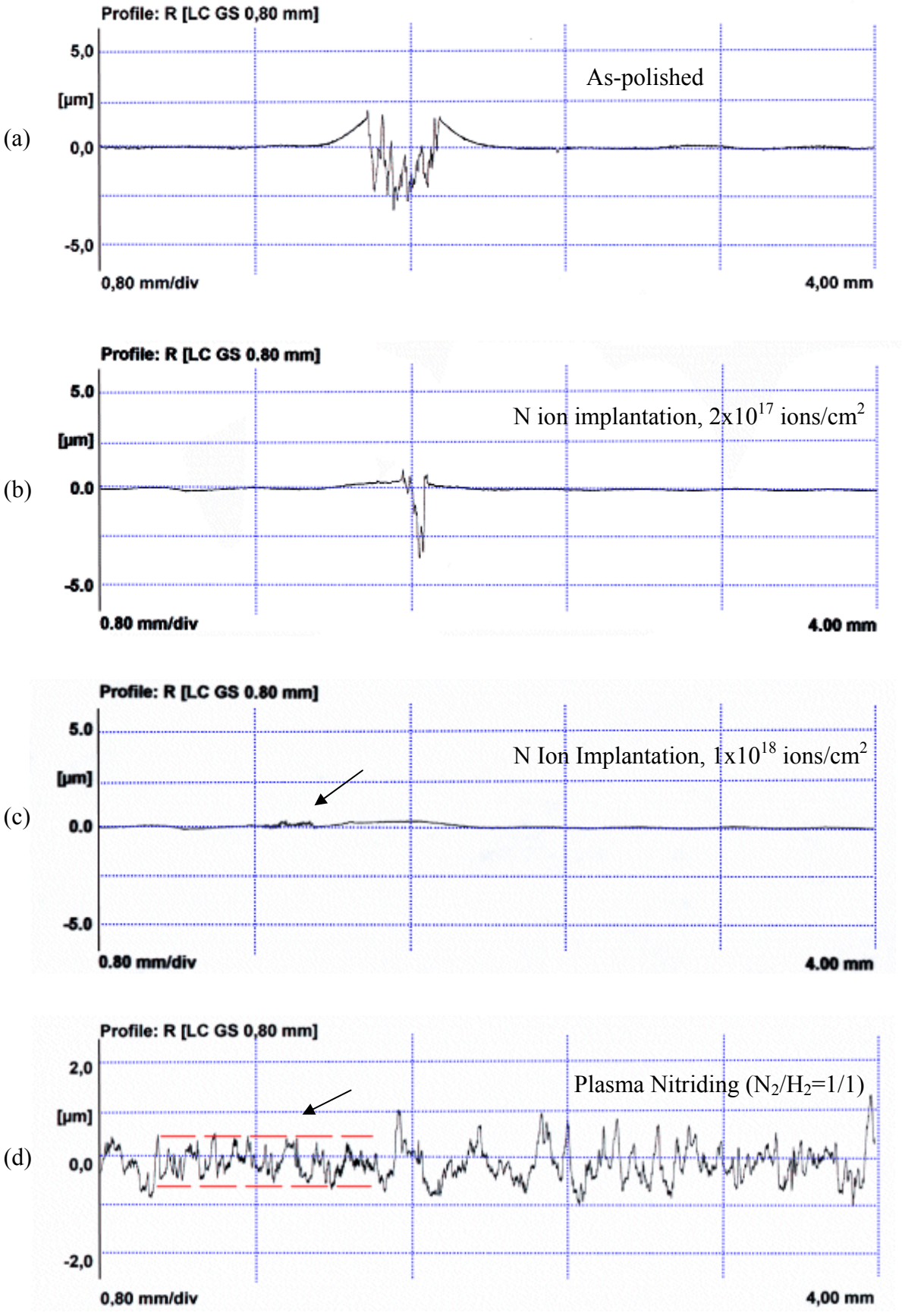

Figure 5.6. Wear trace analysis profiles for the as-polished (the substrate), N ion implanted and the plasma ion nitrided specimen (N_2/H_2=1/1).

5.4 Corrosion Analysis

The salt spray corrosion analysis results are summarized in Table 5.3. As can be seen from this table, the specimen nitrided under the N_2/H_2 = 1/1 plasma nitriding conditions is found to have excellent corrosion resistance compared to the substrate material. The time for the corrosion initiation is greater than 8 hrs for the N_2/H_2 = 1/1 sample while it is only 3 hrs for the as-polished substrate.

The corrosion initiation times, on the other hand, for the specimens nitrided under the N_2/H_2 = 1/10 and 3/1 conditions, are the same, and this value (2 hrs) is even smaller than that of the substrate material indicating poorer corrosion behaviour for these samples.

The best corrosion behaviour is thus obtained for the specimen nitrided under the N_2/H_2 = 1/1 gas flow ratio conditions even though the XRD results for this specimen finds CrN to be one of the phases existing in the top nitrided layers (the compound layer). The enhanced corrosion resistance is attributed to the formation of a well-defined compound layer (see the photomicrographs in Fig. 4.2). Note that the XRD/CEMS/CXMS results for this sample show that the top nitrided layer is rich in ε-nitride phase. The poorer corrosion resistance of the N_2/H_2 = 1/10 and 3/1 specimens can be attributed to the formation of CrN precipitates found to be distributed in the nitrided layers based on the SEM results of the samples. The poorer corrosion results also agree quite well with the etching results for the same specimens.

Table 5.3. The experimental results associated with the salt spray corrosion analysis.

Specimen	Corrosion initiation duration (hour, h)
As-polished	3
Ion nitrided	
1/10	2
1/1	>8*
3/1	2
N ion implanted	
$2x10^{17}$	-
$1x10^{18}$	5

***** Note that this experiment had to be stopped without observing corrosion initiation in 8 hours as explained in Chapter 2.

Table 5.3 also shows the corrosion experiment results for the nitrogen implanted specimens. The data in this table indicates that the high dose N implanted specimen has a very good corrosion behaviour compared to the substrate material. This is attributed to the ε-nitride phase [ε-$(Fe,Cr,Mn)_{2+x}N$] which was found to be distributed in the N implanted layers based on the XRD/GIXRD and CEMS results. This result is also consistent with the literature [22] which shows that the corrosion resistance of iron nitrides are better than ferrite.

After the corrosion initiation occurred, the surface morphologies of the specimens were visually inspected via optical microscope and some pictures of them were taken. The pictures are shown in Fig. 5.7. Due to some technical difficulties however, we were not able to obtain the photographs for the N implanted specimens.

As can be seen from Fig. 5.7, the picture of the N_2/H_2 = 1/1 nitrided specimen shows no corrosion initiation during the course of the corrosion test. However, the photographs for the 1/10 and 3/1 specimens clearly show that the corrosion initiation has taken place for them.

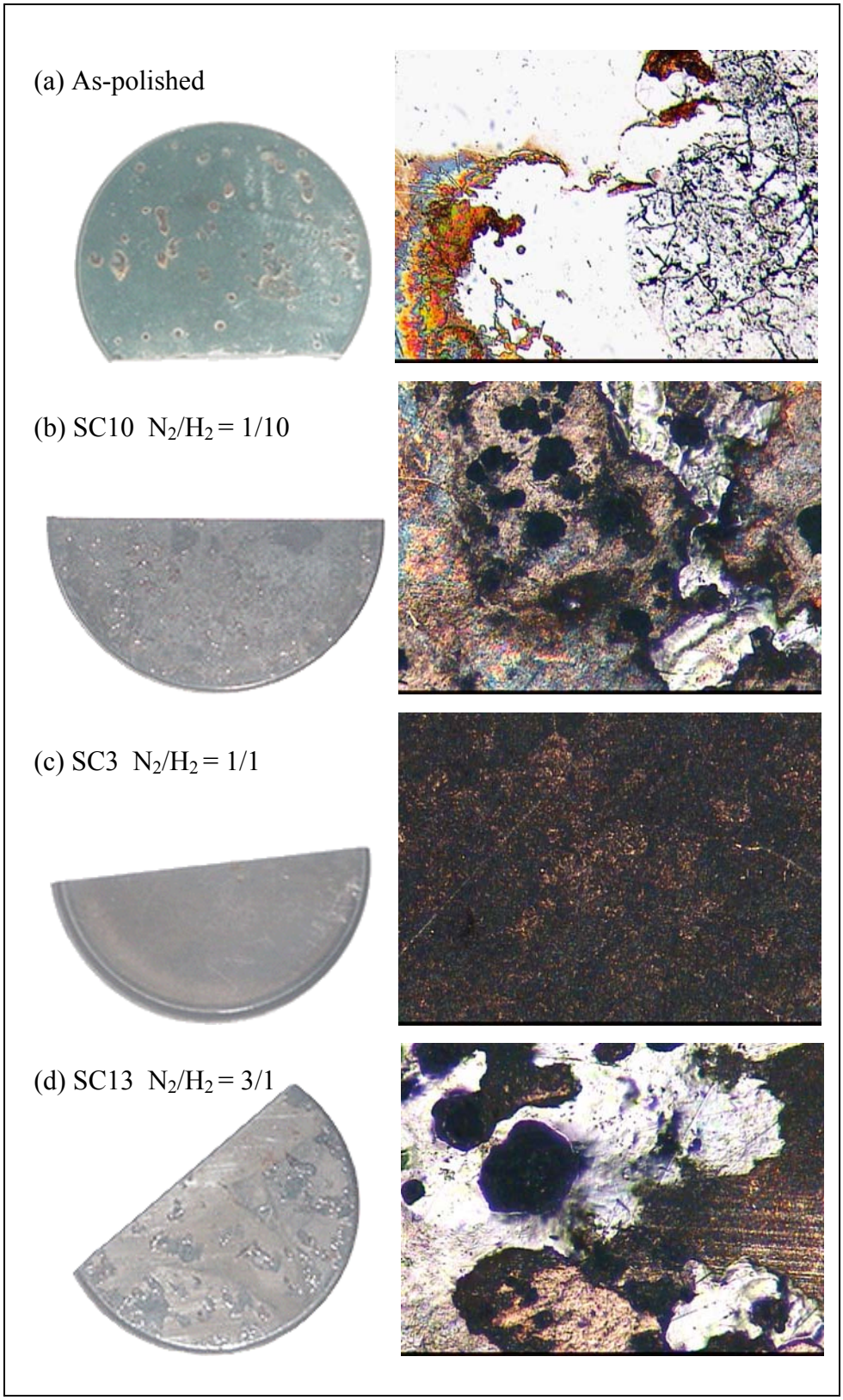

Figure 5.7. Optical micrographs (x100) showing the surface morphologies of the corrosion tested specimens (a) As-polished, (b) $N_2/H_2 = 1/10$, (c) $N_2/H_2 = 1/1$, (d) $N_2/H_2 = 3/1$.

CHAPTER 6

SUMMARY AND CONCLUSIONS

6.1 Summary Discussion

In this study, microstructural and surface mechanical characterization of plasma ion nitrided and nitrogen ion implanted plasma injection mould steel (X36CrMo17 - AISI ~ 420F) were investigated. The experimental results in the preceding chapters clearly show that plasma ion nitriding and nitrogen ion beam implantation lead to the development of various near-surface microstructures and enhanced tribological and mechanical properties of the surface of the plastic injection mould steel.

The effect of varying nitriding gas compositions, N_2/H_2, on the microstructural, mechanical and corrosion characteristics of the plasma nitrided X36CrMo17 used for injection moulds was investigated by means of XRD, CEMS/CXMS, cross-sectional SEM and nanohardness, corrosion testing, and friction and wear analyses.

The experimental SEM and nanohardness-depth results indicate that the nitrided layer thickness is maximized near the N_2/H_2 = 1/1 plasma nitriding conditions and this correlates well with an excellent corrosion behaviour, much increased surface hardness value, and plateau- shaped hardness profile found from the corrosion tests and cross-sectional nanohardness measurements. Under the N_2/H_2 = 1/1 plasma nitriding conditions (a bias voltage of 500 V, nitriding tempratures 540 ˚C, and nitriding time of 18 hrs), combined XRD and Mössbauer analysis results show that ε-$(Fe,Cr,Mn)_{2+x}N$ with x ≈ 1, γ'-$(Fe,Cr,Mn)_4N$, CrN, and the cementite-like [$(Fe,Cr,Mn)_3C$] phases are distributed in the nitrided layer of several micron thickness (~135 μm). In this case, the nitrided layer is found to be composed of the compound and the diffusion layers.

CEMS and CXMS results show the nearly complete decomposition of the substrate layers into pure α-Fe(Mn), ε- and γ'-nitrides, CrN, and the cementite-like phase [$Fe(Cr,Mn)_3C$]. The observation of Fe_3C-like phase is attributed to the near-

surface carbon segregation and/or to the presence of the extra carbon believed to be supplied into the chamber via back streaming from the diffusion pump.

The excellent corrosion behaviour and high acid etch resistance of the nitrided layer is mainly attributed to the ε-nitride phase. The cross sectional nanohardness measurements indicate that the surface layer hardness under all nitriding conditions is increased by about a factor of 3 in comparison to that of the substrate. The enhanced hardness values for the nitrided layers are due to the CrN precipitates (observed by SEM) found to be distributed along the nitrided layer. [It is also assumed that the compressive residual stresses might contribute to the enhanced hardness values.]

The friction and wear analysis results indicate that the coefficient of friction values for the nitrided layers is 20 to 25 % smaller than that of the substrate value. The nitrided layer also shows enhanced wear behaviour and this is attributed to enhanced hardness values for the nitrided layer.

The nitrided layer thicknesses are found to be 20 μm and 40 μm under the N_2/H_2 = 1/10, and 3/1 plasma nitriding conditions, respectively. These values are much smaller than the thickness value (~135 μm) for the N_2/H_2 = 1/1 specimen. This can be explained by the fact that the growth of the nitrided layers are affected by the amount of active nitrogen relative to hydrogen in the plasma (i.e., the concentration of the nitrogen determines the rate of the inward diffusion), and sputtering. The first term has positive effect on the layer growing, while the second term has negative. At high gas flow ratios (i.e., N_2/H_2 = 3/1), thinner nitrided layer forms due to intense sputtering taking place (i.e., the sputter rate becomes comparable to the diffusion rate). And at low gas flow conditions (i.e., N_2/H_2 = 1/10), the formation of thinner nitrided layer can be explained as follows: After the formation of the plasma the active nitrogen starts to diffuse into the surface of the steel. Since the nitrogen concentration is low in the plasma, an equilibrium is reached between the nitrogen in the plasma and the dissolved nitrogen in the surface of the steel. When the equilibrium is surpassed no more nitrogen can be dissolved in the surface of the steel.

In addition to plasma nitriding, nitrogen ion implantation has also been used to investigate microstructural and mechanical properties of X36CrMo17 injection mould steel. Combined XRD and CEMS results show that the plastic injection mould steel implanted with 85 keV N ions to low and high doses of $2x10^{17}$ and $1x10^{18}$ ions/cm^2,

respectively, lead to a hexagonal type ε-nitride phase, [ε-$(Fe,Cr,Mn)_{2+x}N$], with both magnetic (with x~ 0) and paramagnetic (with x~1) characteristics.

Based on the Mössbauer analysis, the N implanted layer thicknesses are about 65 and 40 nm for the high dose and low dose implanted specimens, respectively. Cross-sectional nanohardness and salt spray corrosion analysis indicate that both the high ($1x10^{18}$ ions/cm^2) and low ($2x10^{17}$ ions/cm^2) dose implanted specimens have enhanced hardness and corrosion behaviour. The hardness value for the high dose implanted specimen is found to be increased by about a factor of more than 1.6 compared to the substrate material. The enhanced hardness is attributed to higher N content nature of Fe_2N-like nitride phase, and the thicker implanted layer (~65 nm) for this sample.

The salt spray corrosion analysis results show that the corrosion initiation takes much longer (twice as long) for the N implanted layers in comparison to that of the substrate phase. In addition, based on the SEM sample preparation, the N implanted layers are found to have high acid etch resistance.

The friction and wear experiments show that both the low and high dose N implanted specimens have nearly the same coefficients of friction value (~0.85), which represents about 14 % improvement in comparison to the substrate value (0.99). As for the wear analysis, it is found that the high dose ($1x10^{18}$ ions/cm^2) N implanted specimen has much better wear resistance/behaviour in comparison to both the substrate material and the low dose ($2x10^{17}$ ions/cm^2) N implanted sample.

6.2 Conclusions

(1) (a) Applications of plasma ion nitriding conditions under a bias voltage of 500 V, N_2+H_2 gas mixture ratios from N_2/H_2 = 1/10 to 3/1 for a nitriding temperature of ~530 ˚C lead to ε- and γ'-nitrides, CrN, Fe_3C-like phases in the plasma injection mould steel (X36CrMo17).

(b) Application of nitrogen ion implantation under energies of 85 keV, with a high ($1x10^{18}$ ions/cm^2) and low ($2x10^{17}$ ions/cm^2) dose lead to the formation of [ε-$(Fe,Cr,Mn)_{2+x}N$], phase with both magnetic (with x~ 0) and paramagnetic (with x~1) characteristics.

(2) (a) Nitrided layer thicknesses are in the range of 20 to 135 μm.

(b) N implanted layer has a thickness range of ~ 40-65 nm.

(3) (a) The nitrided layer thickness is found to be maximum near the N_2/H_2 = 1/1 gas flow nitriding conditions and this correlates quite well with an enhanced hardness and excellent corrosion and etch resistance.

(4) Higher N_2/H_2 = 3/1 gas flow conditions results in thinner nitrided layers probably due to the increased sputtering under these conditions.

(5) The coefficient of friction values for the plasma nitrided layers are smaller than those for the N implanted layers.

(6) (a) Plasma nitrided surfaces show improved wear resistance.

(b) The high dose implanted specimen exhibits more enhanced wear resistance compared to the low dose implanted specimen.

6.3 Future work

In this study, high-chromium ferritic plastic injection mould steel (X36CrMo17, similar to AISI-420F) was subjected to plasma nitriding and nitrogen ion beam implantation under various conditions. The effectiveness of conventional plasma nitriding and nitrogen ion beam implantation conditions in improving the tribological properties and mechanical performance was investigated. For a complete understanding of the possible effects of plasma nitriding and nitrogen ion implantation the following studies would be necessary:

(1) In this study, we focused on the extremity gas mixture conditions for plasma nitriding treatments. The gas flow ratios in between these values should be studied to find the best gas flow ratio (N_2/H_2 = 2/10, 3/10, 5/10).

(2) A main drawback of the conventional plasma nitriding is relatively high temperature ranges. In these temperature ranges Cr starts to diffuse from the solid solution and forms nitrides (CrN). This formation of nitride decreases the corrosion resistance of the chromium steels in most cases. To prevent such nitride formation low temperature plasma nitriding ≤450 ˚C should also be investigated.

(3) One of the problems associated with moulds for plastic injection is their birttleness around the edges and the corners. In this study we were not able to

investigate quantitavely the brittleness of the specimens. Therefore, brittleness of the plasma nitrided layer needs to be investigated.

(4) In this study, enhanced hardness values are mainly attributed to the formation of nitrides. A detailed investigation of the residual stress formation and the possible influence on the load bearing capacity and hardness is further needed.

(5) The optimum conditions for the treatments should be tested on the plastic injection moulds.

REFERENCES

[1] E.J. Bienk, N.J. Mikkelsen, "Application of a Advanced Surface Treatment Technologies in Modern Plastic Moulding Industry", *Wear*, **207** (1997) 6-9

[2] C.A Straede, "Application of Ion Implantation in Tooling Industry", *Nuclear Instruments and Methods in Physics Research* B, **113** (1996) 161-166

[3] N.J. Mikkelsen, J. Pedersen, C.A Straede, "Ion Implantation-the Job Coater's Supplement to Coating Techniques", *Surface and Coatings Technology*, **158/159** (2002) 42-47

[4] R.J. Rodrígues, A. Medrano, M. Rico, R. Sánchez, R. Martínez, J.A. García, "Niche Sectors for Economically Competitive Ion Implantation Treatments", *Surface and Coatings Technology*, **158/159** (2002) 48-53

[5] P. C. Jindal, "Ion Nitriding of steels", *Journal of Vacuum Science Technology*, Vol. **15**, No.2, March\April (1978)

[6] M. Berg, C.V. Budtz-Jϕrgensen, H. Resitz, K. O. Schweitz, J Chevallier, P. Kringhϕj, J. Bϕttiger, "On Plasma Nitriding of Steels", *Surface and Coatings Technology*, **124**, (2000) 25-31

[7] H.C.F. Rozendaal, E.J. Mittemeijer, P.F. Colijn, P.J. Van Der Schaaf, "The Development of Nitrogen Concentration profiles on Nitriding Iron", *Metallurgical Transactions A.*, Vol. **14**A, March (1983) 395

[8] M.A.J. Somers, E.J. Mittemeijer, "Layer Growth Kinetics On Gaseous Nitriding of Pure Iron: Evaluation of Diffusion Coefficients for Nitrogen in Iron Nitrides", *Metallurgical and Materials Transactions A.*, Vol. **26A**, (1995) 57

[9] N.L. Loh, L.W. Siew, "Residual Stress Profiles of Plasma Nitrided Steels", *Surface Engineering*, **15** (1999) 137

[10] Y. Sun, T. Bell, "A Numerical Model of Plasma Nitriding of Low Alloy Steels", *Materials Science and Engineering*, **A224** (1997) 33-47

[11] J.Q. Xiao, C.L. Chien, "Radio Frequency Reactive Sputtered Iron Nitrides Using Ammonia Gas: Structure and Magnetic Properties", *Applied Physics Letters*, **64** (3), January (1994) 384-386

[12] D. H. Jack, K. H. Jack, "Invited Review: Carbides and Nitrides in Steel", *Materials Science and Engineering*, **11** (1973) 1-27

[13] Nitrion GmbH, Nitrierbetriebe Bayern, "*Plasma Nitriding in Comparison with Gas Nitriding*" Technical Report

[14] S.Kumar, M.J. Baldwin, M. P. Fewell, S.C haydon, K.T. Short, G.A. Collins, J. Tendys, "The Effect of Hydrogen on the Growth of Nitrided Layer in r.f.-Plasma-Nitrided Austenitic Stainless Stell AISI 316", *Surface and Coatings Technology*, **123** (2000) 29-35

[15] M. Karakan, A. Alsaran, A. Çelik, "Effects of Various Gas Mixtures on Plasma Nitriding of AISI 5140 Steel", *Materials Characterization*, **49** (2003) 241-246

[16] C. Blawert, B.L. Mordike, U. Rennsch, R. Wünsch, R. Wiedemann, H. Oettel, "Influence of the Material Composition on the Nitriding Result of Steels by Plasma Immersion Ion Implantation", *Surface and Coatings Technology*, **131** (2000) 334-339

[17] Materials Science and Technology, A Comprehensive Treatment" edited by R.W. Chan, P. Haassen, E.J. Kramer, Vol. **15**, *Processing and Metals and Alloys*, Page 249

[18] A. Jr Clodomiro, J. de Anchieta Rodrigues, A.E. Martinelli, "Growth of Nitrided Layers on Fe-Cr Alloys", *Materials Science and Engineering*, A **279** (2000) 10-15

[19] C. E. Pinedo, W. A. Monterio, "Surface Hardening by Plasma Nitriding on High Chromium Steel", *Journal of Materials Science Letters*, **20** (2001) 147-149

[20] K. Marchev, C.V. Cooper, B. C. Giessen, "Observation of Compound Layer with Very Low Friction Coefficient in Ion-Nitrided Martensitic 410 Stainless Steel", *Surface and Coatings Technology*, **99** (1998) 229-223

[21] M.U. Devi, T.K. Chakraborty, O.N. Mohanty, "Wear Behaviour of Plasma Nitrided Tool Steels", *Surface and Coatings Technology*, **116/119** (1999) 212-221

[22] T. Michler, M. Grische, K. Bewilogua, H. Dimigen, "Properties of Duplex Coatings Prepared by Plasma Nitriding and PVD Ti-C:H deposition on X20Cr13 Ferritic Steel", *Thin Solid Films*, **322** (1998) 206-212

[23] R. Wei, P. J. Wilbur, W.S. Sampath, D.L Williamson, Li Wang, "Sliding Wear of Nitrogen Ion-Implanted Stainless Steels", *Lubrication Engineering*, **47** 4 (1991), 326-334

[24] R. Wei, P. J. Wilbur, O. Öztürk, D.L Williamson, "Tribological Studies of Ultrahigh Dose Nitrogen-Implanted Iron and Stainless Steel", *Nuclear Instruments and Methods in Physics Research,* B **59/60** (1991) 731-736

[25] Y. Miyagawa, S. Nakao, M. Ikeyama, K. Saitoh, S. Miyagawa, "Saturated Thickness of Nitride Layers Formed by High Fluence Nitrogen Implantation into Metals", *Nuclear Instruments and Methods in Physics Research*, B **127/128** (1997) 765-769

[26] L.D. Yu, T. Vilaithong, D. Suwannakachorn, S. Intarasiri, S. Tongtem, "Ion Implantation Modification of Special Steels in Tailand", *Nuclear Instruments and Methods in Physics Research*, B **127/128** (1997) 954-960

[27] D.L. Williamson, Li Wang, R. Wei, P.J. Wilbur, "Solid Solution Strengthening of Stainless Steel Surface Layers by Rapid, High Dose, Elevated Temperature Nitrogen Ion Implantation", *Materials Letters*, Vol.**9**, Number 9, May (1990) 302-308

[28] G.W. Malaczynski, C.H. Leung, A.A. Elmoursi, A.H. Hamdi, A.B. Campbell, M.P. Balogh, M.C. Militello, S.J. Simko, R.A. Waldo, "Characterization of Surface Modified α-Iron by Nitrogen Plasma Immersion Ion Implantation: A Microstructural Study", *Materials Science and Engineering*, A**262** (1999) 289-299

[29] X.B. Tian, Z.M. Zeng, B.Y. Tang, T.K. Kwok, P.K. Chu, "Fast Pulsing Plasma Immersion Ion Implantation for Tribological Applications", *Surface and Coatings Technology*, 128-129 (2000) 226-230

[30] D.L. Williamson, O. Öztürk, S. Glick, R.Wei, P.J. Wilbur, "Microstructure of Ultrahigh Dose Nitrogen-Implanted Iron and Stainless Steel", *Nuclear Instruments and Methods in Physics Research*, B **59/60** (1991) 737-741

[31] P. Budzyński, P. Tarkowski, P. Penkala, "The Influence of Nitrogen Ion Implantation on Tribological Properties of Tool Steel NC10", *Vacuum*, **63** (2001) 731-736

[32] J.Sasaki, M Iwaki, "Frictional properties and micro-characteristics of N2+-implanted Fe-Cr alloys with various chromium contents", *Thin Solid Films,* **201** (1991) 39-48

[33] G.M. Methora, V.K. Jean, H.M. Urdianyk, B.D Barton, "Effect of ion implantation on friction and wear behavior of steels", *Wear*, **159** (1992) 47-55.

[34] F.G. Yost, S.T. Piraux, D.M. Follstaedt, L.E. Pope, J.A. Knapp, "The effects of N+ implantation on the wear and friction of type 304 and 15-5 PH stainless steels" Thin *Solid Films,* **107** (1983), 287-295

[35] A. M. Kliauga, M. Pohl, D. Klaffke, "A Comparison of the Friction and reciprocating Wear Behaviour Between an Austenitic (X 2 CrNiMo17 13 2) and a Ferritic (X 1 CrNiMoNb28 4 2) Stainless Steel After nitrogen Ion Implantation", *Surface and Coatings Technology*, **102** (1998) 237-244

[36] G. Thorwarth, S. Mändl, B. Rauschenbach, "Plasma Immersion Ion Implantation of Cold-Work steel", *Surface and Coatings Technology*, **125** (2000) 94-99

[37] G. Collins, "New applications for Plasma Nitriding", Technical Article, *Materials Australia*, May/June (1999) 18-21

[38] W.L. Li, W.D. Fei, Y. Sum, "Grazing-Incidence X-Ray Scattering and Diffraction Study of the Nitrogen Ion Implantation Layer Produced by Plasma-Based Ion Implantation", *Surface and Coatings Technology*, **150** (2002) 64-69

[39] "*ASM Handbook*", Vol.9, "*Metallography and Microstructures*", Page 71

[40] L. Abada, G. Rixerceri, F. Aubertion, P. Schaaf and U. Gonser, "Information Depths of Conversion X-ray Mössbauer Spectra in Plasma Nitrocarburized Surface Layers", *Phys. Stat. Sol*., (a), **139** 181 (1993)

[41] O. Öztürk, "*Surface Modification of Austenitic Stainless Steels by High-flux elevated Temperature Nitrogen-Ion Implantation*" Dissertation, Colorado School of Mines, T-4489 (1994)

[42] N. Renevier, T. Czerwiec, A. Billard, J. von. Stebut, H. Mitchel, "A Way to Decrease the Nitriding Temperature of Aluminium: The Low-Pressure Arc-Assisted Nitriding Process", *Surface and Coatings Technology*, **116/119** (1999) 380-385

[43] B. Larish, U. Brusky, H.J. Spies, "Plasma Nitriding of Stainless Steel at Low Temperatures", *Surface and Coatings Technology*, **116/119** (1999) 205-211.

[44] C.F.M Borges, S. Hennecke, E. Pfender, "Decreasing Chromium Precipitation in AISI 304 Stainless Steel During the Plasma-Nitriding Process", *Surface and Coatings Technology*, **123** (2000) 112-221

[45] M.J. Baldwin, M.P. Fewell, S.C Haydon, S. Kumar, G.A. Collins, K.T. Short, J. Tendys, "Rf-Plasma Nitriding of Stainless Steel", *Surface and Coatings Technology*, **98** (1998) 1187-1191

[46] B. D. Cullity, "*Elements of X-Ray Diffraction*" Addison-Wesley Publishing Company, Inc. 1978

[47] Physics Stat. Solidi., **39** (1970) 121

[48] G. M. Chen, N. K. Jaggl, J. B. Butt, E. Yeh, L. H. Schwartz "Mössbauer and Magnetic Studies of ε-Fe_xN, $2<x<3$", *Journal of Physics and Chemistry*, **87** (1983) 5326-5332

[49] D. L. Williamson, F. M. Kustas, D. F. Fobare, M. S. Misra, "Mössbauer study of Ti-implanted 52100 steel", *Journal of Applied Physics letters*, **60** (1986) 1493

[50] J.F. Ziegler, J.P.Biersack, U.Littmark, "The Stopping and Range of Ions in Solids", Pergamon Press, New York, 1985, Vol.1 [TRIM version 91.14 used here]

[51] O. Öztürk, D.L. Williamson, "The Annealing Behaviour of Nitrogen in fcc Stainless Steel", *Hyperfine Interactions,* **92** (1994) 1329-1337

[52] O. Öztürk, D.L. Williamson, "Phase and Composition Depth Distribution Analyses of Low Energy, High Flux N Implanted Stainless Steel", *Journal of Applied Physics*, **77** (8), April (1995), 3839-3849

[53] D.L. Williamson, O. Öztürk, R. Wei, P.J. Wilbur, "*Metastable Phase Formation and Enhanced Diffusion in f.c.c Alloys under High Dose, High Flux Nitrogen Implantation at High and Low ion Energies*", Surface and Coatings Technology, 65 (1994) 15-23

[54] Yu.P. Sharkeev, E.V. Kozlov, "The Long Range Effect in Ion Implanted Metallic Materials: Dislocation Structures, Properties, Stresses, Mechanisms", *Surface and Coatings technology*, **158/159** (2002) 219-224